CENTRAL RESEARCH LIBRARY
DOCUMENT COLLECTION

2

MARTIN MARIETTA ENERGY SYSTEMS LIBRARIES
3 4456 0286441 6

ORNL-3439
UC-38 - Engineering and Equipment

HEAT TRANSFER FROM SPENT REACTOR FUELS DURING SHIPPING: A PROPOSED METHOD FOR PREDICTING TEMPERATURE DISTRIBUTION IN FUEL BUNDLES AND COMPARISON WITH EXPERIMENTAL DATA

J. S. Watson

CENTRAL RESEARCH LIBRARY
DOCUMENT COLLECTION
LIBRARY LOAN COPY
DO NOT TRANSFER TO ANOTHER PERSON
If you wish someone else to see this document, send in name with document and the library will arrange a loan.

OAK RIDGE NATIONAL LABORATORY
operated by
UNION CARBIDE CORPORATION
for the
U.S. ATOMIC ENERGY COMMISSION

Printed in USA. Price: $1.75 Available from the
Office of Technical Services
U. S. Department of Commerce
Washington 25, D. C.

LEGAL NOTICE

This report was prepared as an account of Government sponsored work. Neither the United States, nor the Commission, nor any person acting on behalf of the Commission:

A. Makes any warranty or representation, expressed or implied, with respect to the accuracy, completeness, or usefulness of the information contained in this report, or that the use of any information, apparatus, method, or process disclosed in this report may not infringe privately owned rights; or

B. Assumes any liabilities with respect to the use of, or for damages resulting from the use of any information, apparatus, method, or process disclosed in this report.

As used in the above, "person acting on behalf of the Commission" includes any employee or contractor of the Commission, or employee of such contractor, to the extent that such employee or contractor of the Commission, or employee of such contractor prepares, disseminates, or provides access to, any information pursuant to his employment or contract with the Commission, or his employment with such contractor.

ORNL-3439

Contract No. W-7405-eng-26
Chemical Technology Division

HEAT TRANSFER FROM SPENT REACTOR FUELS DURING SHIPPING: A PROPOSED METHOD FOR PREDICTING TEMPERATURE DISTRIBUTION IN FUEL BUNDLES AND COMPARISON WITH EXPERIMENTAL DATA

J. S. Watson

Date Issued

MAY 27 1963

OAK RIDGE NATIONAL LABORATORY
Oak Ridge, Tennessee
operated by
UNION CARBIDE CORPORATION
for the
U. S. ATOMIC ENERGY COMMISSION

MARTIN MARIETTA ENERGY SYSTEMS LIBRARIES

3 4456 0286441 6

CONTENTS

Page

Abstract 1

1. Introduction 2
   1.1 The Problem: Insufficient Experimental Data and Inadequate Methods for Predicting Heat Transfer from Spent Fuel Pins to the Inner Wall of Air-Filled Shipping Casks. 2
   1.2 Proposed Solution: The Objective of this Study 3

2. Experimental Procedure for Measuring the Temperature Rise in Mock Elements in Simulated Shipping Casks. 4
   2.1 Design of the Mock Fuel Bundles 4
   2.2 Design Compromises and Magnitude of Temperature Errors. 4
   2.3 Assembly of the Mock Fuel Bundles 6
   2.4 Simulation of Shipping Casks. 6
   2.5 Recording the Temperatures and Determining the Heat Generation Rates. 11
   2.6 Measurement of the Emissivity of the Stainless Steel Tubes Used in the Bundles 11

3. Mathematical Development of Method for Predicting Temperature Distribution 12
   3.1 Introduction. 12
   3.2 Evaluation of Radiation Configuration Factors for Long, Parallel Tubes. 12
      3.2.1 Configuration Factors for Adjacent Tubes . . . 14
      3.2.2 Configuration Factors for Diagonally Located Tubes. 18
      3.2.3 Configuration Factors for Radiation Between Tubes Further Separated in the Array 24
   3.3 Estimation of Grey-Body Radiation Factors 27
   3.4 Predictions of the Temperature Distributions within Fuel Bundles: A Proposed Method. 29

4. Results. 30

5. Conclusions and Recommendations. 62

6. References 62

7. Appendix: FORTRAN Code. 62

HEAT TRANSFER FROM SPENT REACTOR FUELS DURING SHIPPING: A PROPOSED METHOD FOR PREDICTING TEMPERATURE DISTRIBUTION IN FUEL BUNDLES AND COMPARISON WITH EXPERIMENTAL DATA

J. S. Watson

ABSTRACT

A simple method has been developed for calculating or predicting temperature distributions in spent reactor fuels in shipping casks. The method accounts for radiant heat transfer between all the individual pins in a square array. With the dimensions of the fuel bundle, the configuration factors for radiation between various tubes in the bundle can be obtained from tabulated numerical calculations presented in this report. The configuration factors, along with the heat generation rates, surface emissivity, and the temperature of the wall of the cask can be used to estimate the temperature distribution automatically with a computer code presented in this report or possibly by hand calculations by the method outlined.

Experimental measurements of temperature distribution in electrically heated tube arrays in steel shells that simulated shipping casks were made to test the proposed calculational procedure. Several heat generation rates and bundles containing up to 64 tubes were tested in 12-in.- and 6-in.-inner diameter shells. Tests were made with the casks in horizontal and vertical positions. The predicted temperatures were very near those observed experimentally under the conditions in which heat transfer is likely to be a problem in fuel shipment, that is, when the temperatures are near or above 200°C and the casks do not contain large empty spaces. These are the conditions where radiation should be expected to be the most important mechanism.

The calculational method may also be adapted to nonsquare arrays.

1. INTRODUCTION

1.1 The Problem: Insufficient Experimental Data and Inadequate Numerical Methods for Predicting Heat Transfer from Spent Fuel Pins to the Inner Wall of Air-Filled Shipping Casks

The removal of radioactive decay heat from spent reactor fuels is one of the major problems encountered during shipment of these fuels from the reactor to the processing site. Because of the thick radiation shields required around the fuel elements and the sizeable heat generation rates involved, the temperatures of the fuel pins will be considerably above that of the surrounding atmosphere. In order to avoid melting the fuel or causing any other damage that could result in the release of radioactive materials or otherwise endanger the surroundings, the fuel carrier must be designed to maintain these temperatures within safe limits under any credible set of conditions. However, it is also desirable to keep shipping costs as low as possible through economic carrier design and shipping schedules. Since the rate of heat removal may limit the capacities of many carriers handling the proposed highly burned power reactor fuels, accurate methods of predicting temperature rises are needed for safe yet low-cost carrier design and use.

The removal of heat from a cask can usually be enhanced considerably by circulating a liquid heat transfer medium (e.g., water) through the cask by either forced or natural convection. The liquid may be cooled by an external heat exchanger, or it may simply aid in transferring heat from the fuel to the inner wall of the cask. Although liquid coolants will probably be useful, especially in larger casks, in holding down fuel temperatures, one must never forget the possibility of an accident during shipment, in which the liquid is lost. Efforts are being made by several groups to determine (1) the maximum credible accident which could be expected during shipment, (2) the structural properties that a cask will need to withstand such an accident, and (3) what types or degrees of damage can be suffered by the cask without overly endangering the surroundings. Although shipping standards are not firmly established, it does not appear likely that one can rely upon a reasonably designed cask

to maintain its liquid coolant during a serious accident. Although liquid coolants are used, the cask should be designed so that the heat can be removed without seriously damaging the fuel even when air is the only heat transfer medium available.

Experimental data and methods of predicting heat transfer rates from the spent fuel element to the inner wall of air-filled casks appear to be the greatest general needs in shipping cask design. Although heat transfer with liquid coolants inside the cask, the effectiveness of metal-metal bonds, and the use of exterior fins are all interesting problems of cask design, in many ways they appear more like specific problems of individual casks. Heat transfer from the fuel to the cask wall without liquid coolant is a problem of interest in all cask designs.

1.2 Proposed Solution: The Objective of this Study

The objective of this study is to help fill the need discussed above by providing experimental data on the temperature rise in a few fuel-and-cask configurations and to present a conservative method for predicting the temperatures within the fuel element that are consistent with these experimental data. Although it will probably long remain advisable to test the heat transfer capabilities of a cask and fuel before service, it still remains necessary to constantly search for better methods of predicting these properties so that the original cask design can be made closer to the optimal design for the desired service and so that more accurate and rapid estimates of fuel shipping costs can be made.

The present study was limited to what appeared to be the most commonly proposed power reactor fuel element shape: square-pitched bundles of long tubes. Although several fuels, especially those of small reactors, are of the plate type, the bulk of the nonmilitary reactors will be fueled with bundles of fuel tubes.

2. EXPERIMENTAL PROCEDURE FOR MEASURING THE TEMPERATURE RISE IN MOCK ELEMENTS IN SIMULATED SHIPPING CASKS

2.1 Design of the Mock Fuel Bundles

To measure the temperature rise expected in spent power reactor fuel elements during shipment, mock fuel bundles were made from 5/16-in.-ID stainless steel tubes, as shown in Fig. 1. The tubes were heated electrically (rather than by radioactive-decay heat) by a Nichrome wire running through ceramic insulators inside the tube. The temperature of the surface of the tube was measured by 1/16-in.-sheathed Chromel-Alumel thermocouples, also inserted into the tube.

2.2 Design Compromises and Magnitude of Temperature Errors

In designing these fuel tubes, the usual conflict between accuracy of the results and economy of fabrication and ease of use was encountered. In this case extreme accuracy was not warranted, and the relatively simple design described above was chosen. This system violates several principles of good temperature measurements, but it appeared to give reproducible temperatures accurate to within about 2 or 3°C. Since the temperature of interest was that of the outside of the tube wall, it would have been desirable to have the measuring thermocouple welded to the outside of the tube and to have the heat source (resistance-heating wires) exactly in the center of the tube. In many of the fuel elements of interest, the spacing between the fuel tubes is so small that if the thermocouples had been attached to the outside of the tube, it would need to be essentially flush with the wall, and the leads would need to be withdrawn through the inside of the tube. Such a system would be capable of good accuracy, but the tubes would be quite expensive to make. The simpler system actually used should always be expected to read high, but it was easy to assemble, and a single thermocouple could be used to measure the temperature at several points along the length of the tube by simply removing or inserting it further into the tube.

Since almost all heat transfer inside the tube is by conduction, the errors involved in the temperature measurements should be proportional

UNCLASSIFIED
ORNL-LR-DWG 59755

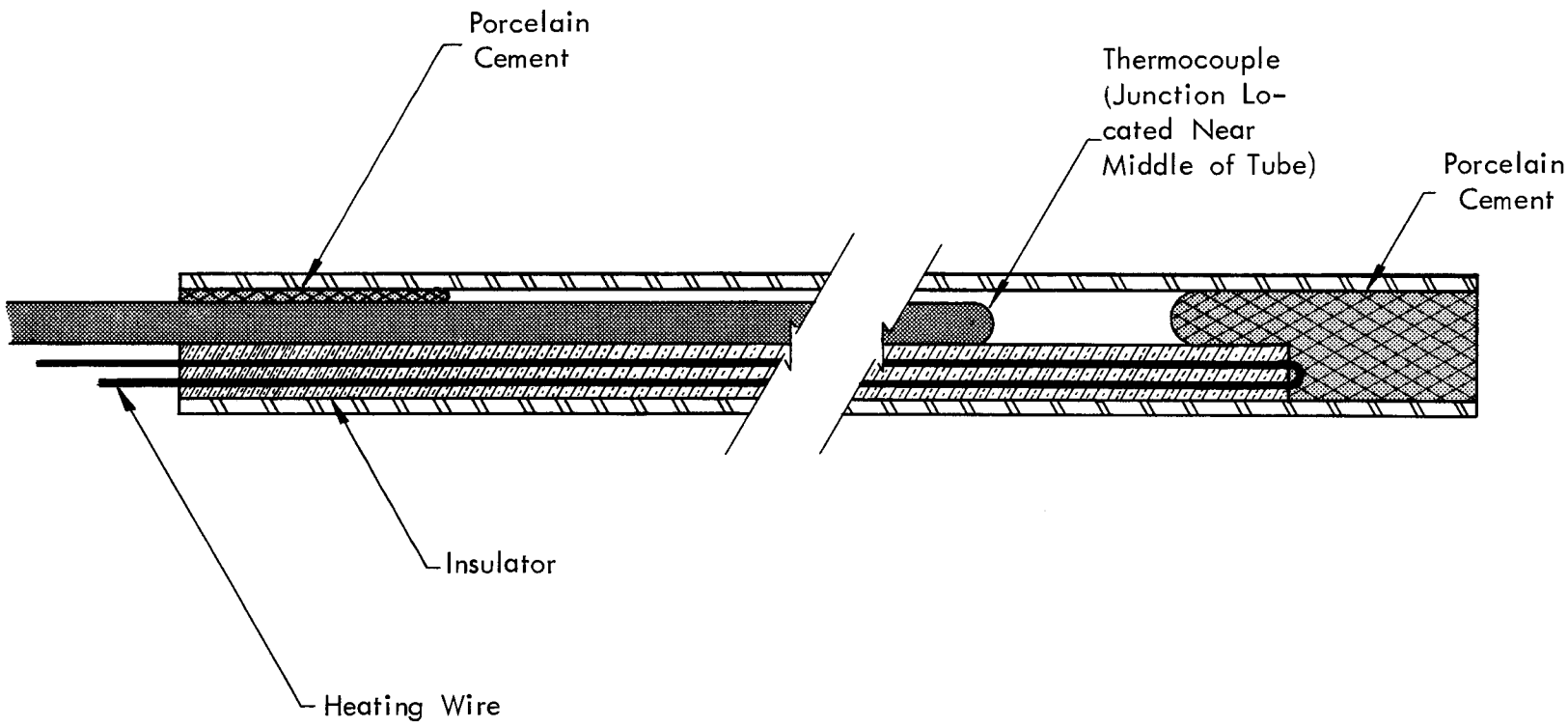

Fig. 1. Cross Section of Mock Fuel Pin.

to the heat flux through the thermocouple or the heat generation rate in the tube. During a brief series of heat transfer measurements through a packed granular bed, a test of this error was made. A thermocouple was welded on the side of one of the fuel tubes, and another thermocouple was placed inside the tube, as shown in Fig. 1. The tube was placed in the center of a 3-in. pipe and the annular space filled with steel shot. The tube was then heated at various heat generation rates and readings taken from both thermocouples. The difference between the two readings, as noted earlier, was a linear function of the heat generation rate. In this case rather large heat generation rates could be used (See Fig. 2). When these results are extrapolated down to the heat generation rates used in the cask tests, they indicated that the errors should be less than 3°C.

2.3 Assembly of the Mock Fuel Bundles

In assembling these tubes into simulated fuel assemblies, spacers were required to hold the fuel tubes apart a specified distance. In actual fuel elements, small metal rings and/or spiral wires are usually attached to the tubes for this purpose. These rings can aid in heat transfer through the bundle, but since the heat transfer through these spacers will be different for different reactor fuels, it was considered desirable in this study to minimize this heat transfer so the results would more nearly approach the worst case. "Lavite" was the most satisfactory spacing material tried. In order to simplify the assembling of large bundles and connecting power leads, the tubes were first assembled into sub-bundles of four tubes each. Figures 3 and 4 show such sub-bundles with the "Lavite" spacers. The tubes in each sub-bundle were wired in series, and the various sub-bundles in the fuel array could then be connected either in parallel or series for the experiments. The spacers also served to keep the sub-bundles the proper distance apart in the final array.

2.4 Simulation of Shipping Casks

The assembled bundles were heated in stainless steel shells such as the one shown in Fig. 5. These shells were used to simulate the heavy

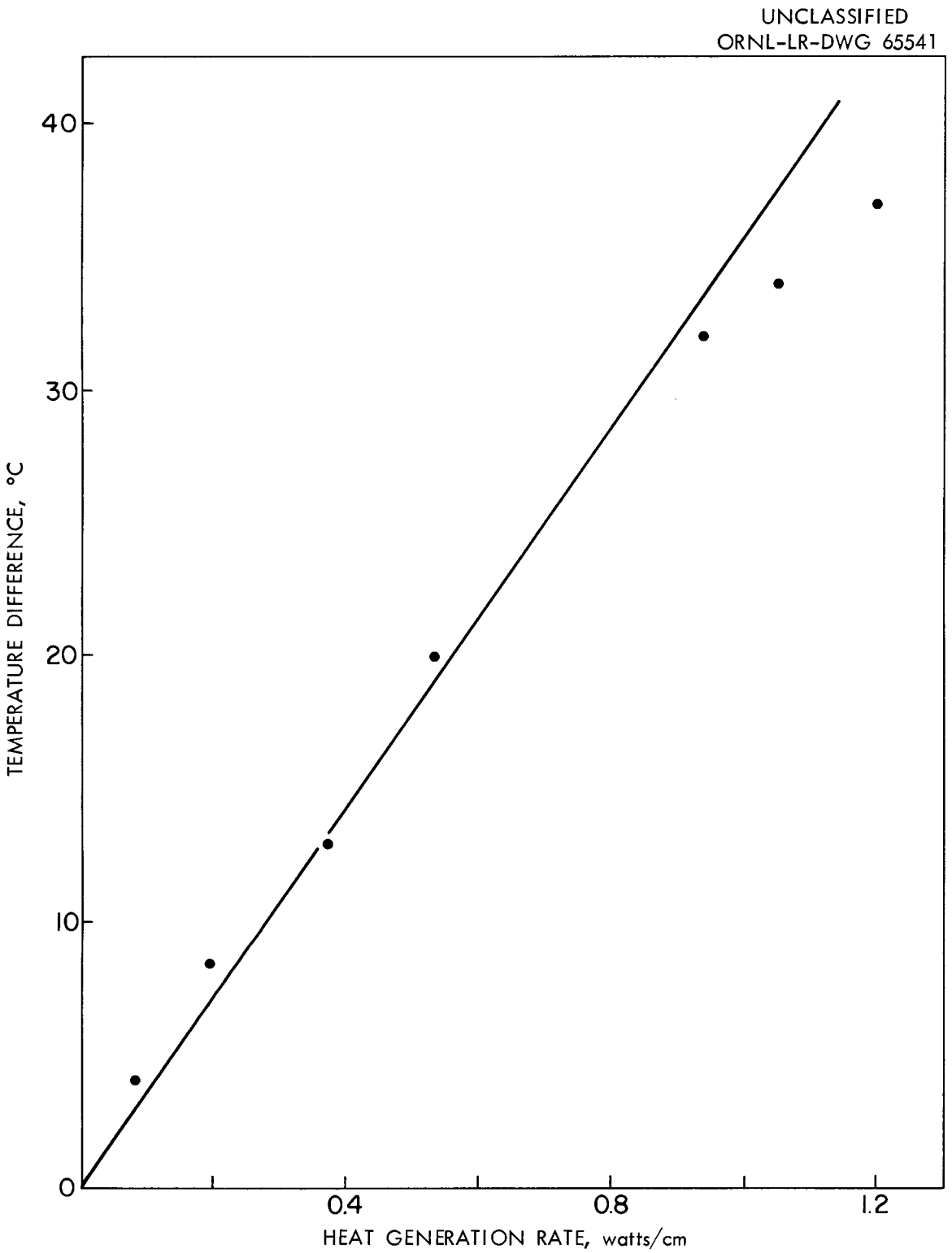

Fig. 2. Difference between Temperatures Measured Inside and on the Surface of Simulated Fuel Tube.

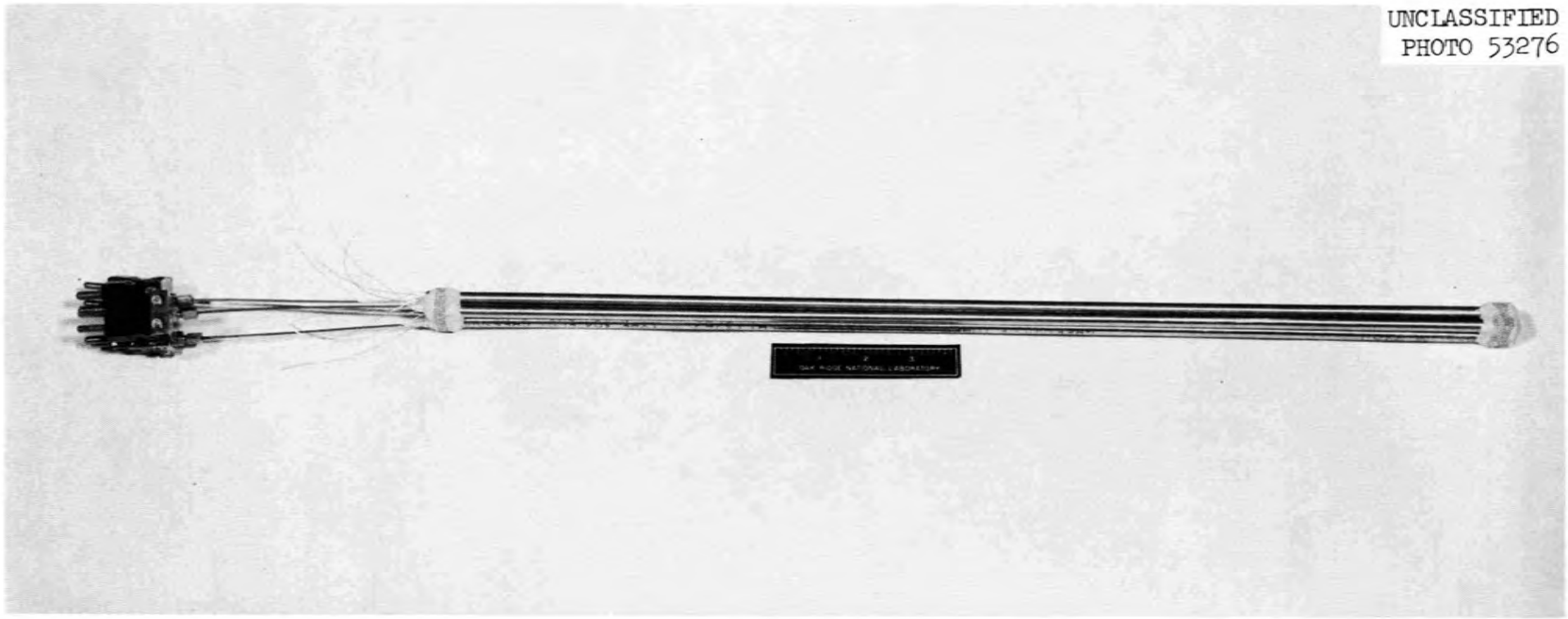

Fig. 3. Sub-bundle of Mock Fuel Element.

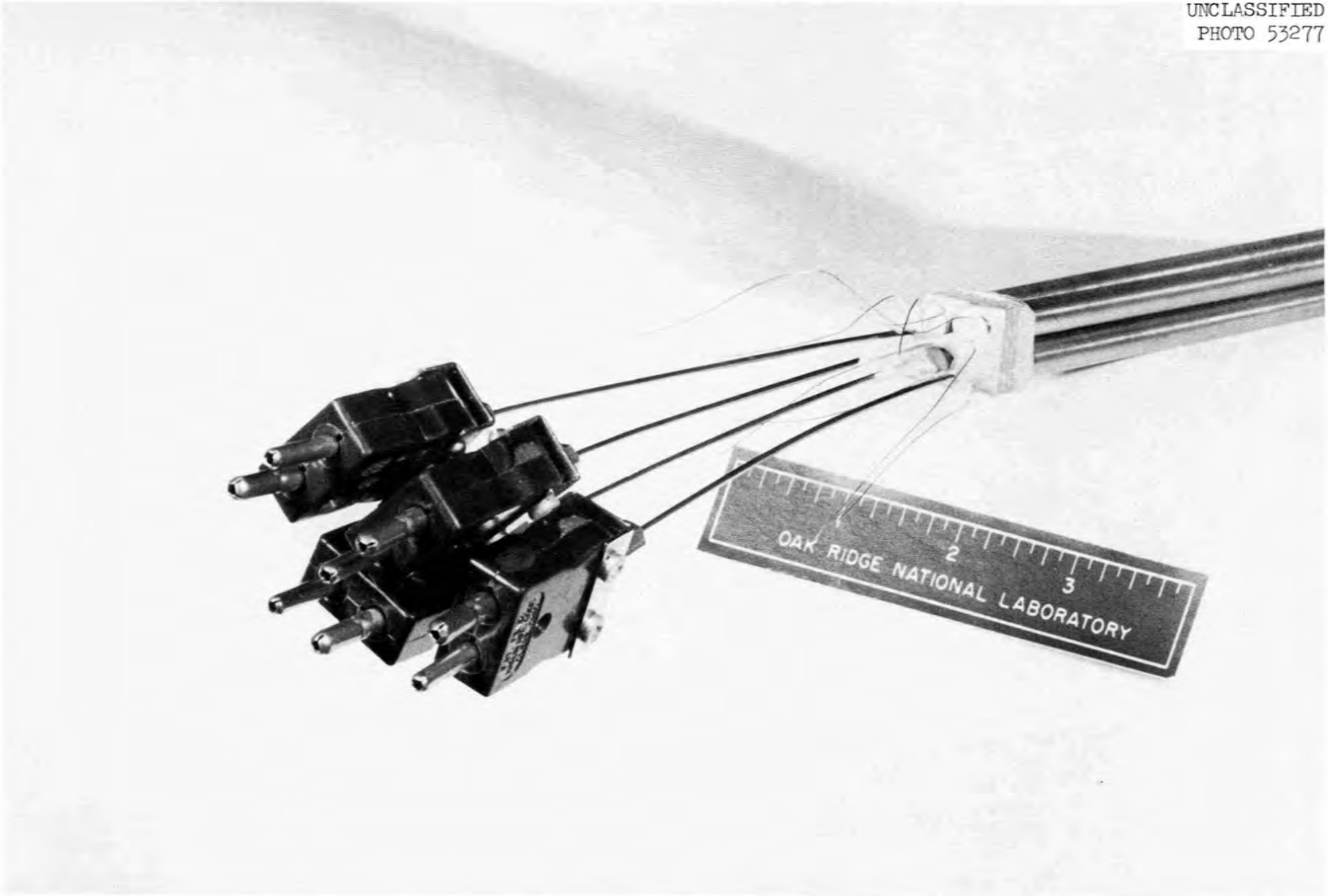

Fig. 4. Thermocouple and Power Leads to Sub-bundle of Mock Fuel Element.

Fig. 5. Fuel Sub-bundle and Container.

lead casks. Various thicknesses of asbestos insulation were wrapped around the shell to simulate various thicknesses of lead shielding on the cask. This arrangement was very good for simulating the resistance of radial heat transfer, but an actual cask should be much more capable of conducting heat around the cask wall. Therefore, these experiments showed more angular dependence of the temperature of the inner wall of the cask than one would expect in an actual cask. However, the relatively thin shells used were much cheaper to make and easier to work with because they had much less heat capacity, thereby permitting steady-state temperature distributions to be reached quickly.

The bundles and simulated casks used were only two feet long. This is much shorter than most power reactor fuel elements will be, but efforts were made to make the results resemble so far as possible much longer systems. The ends of the simulated casks were always insulated with "Transite" (always better insulated than the walls) to reduce the heat transferred out the ends. Also, the Transite surface at the end of the cask was light-colored and appeared to be more reflective than the stainless steel surfaces. Some thermocouples were moved plus or minus 6 in. from the center of the bundle, and when the cask was in a horizontal position, the temperature variation appeared to be negligible.

2.5 Recording the Temperatures and Determining the Heat Generation Rates

The temperatures in selected tubes were recorded to determine the time required to reach steady state, but all steady-state temperatures were read from a Brown precision temperature indicator. The heat generation rate was determined simply by the voltage applied to the sub-bundles and the measured resistance of the sub-bundles. The resistances of all sub-bundles appeared to be practically the same.

2.6 Measurement of the Emissivity of the Stainless Steel Tubes Used in the Bundles

The emissivity of one of the stainless steel tubes was measured by inserting it into the center of a similar stainless steel tube 1 in. in diameter by measuring heat fluxes between the tubes. The annulus between

the two tubes was evacuated, and the center tube was heated at a known rate. The surfaces were assumed to be approximate infinite planes and the emissivity calculated. The pressure in the annular space was lowered until reproducible values were obtained. Below 200 μ Hg, the emissivity calculated was almost constant at 0.55.

3. MATHEMATICAL DEVELOPMENT OF METHOD FOR PREDICTING TEMPERATURE DISTRIBUTION

3.1 Introduction

As in any heat transfer problem the heat generated in the fuel bundle can reach the walls of the cask by conduction, convection, and radiation. In these cases where high temperatures are involved and only atmospheric air with no forced circulation is available as a heat transfer medium, radiation can be expected to be at least one of the significant heat transfer processes. Therefore, the initial analytical effort was directed toward predicting the thermal fluxes due to radiation, and, later efforts, if necessary, were planned to correlate the additional heat transfer which would be due to convection and partially to conduction. However, although there was clear evidence that there was some convection, the temperature distributions under the conditions of most interest were very close to those predicted on the basis of radiation alone. The approximations made in the radiation analysis were probably of the same magnitude as the effects of convection and conduction. This relatively simple calculational procedure for predicting temperature distributions with only radiant heat transfer was considered likely to be more useful than more exact but more difficult or complicated procedures accounting for convection. The system, however, breaks down at low temperatures and in casks with large void spaces, where convection can become important.

3.2 Evaluation of Radiation Configuration Factors for Long, Parallel Tubes

The flow of radiant heat from one black body to another is given by the Stefan-Boltzmann equation:

$$q_{12} = A_1 F_{12} \sigma \quad (T_1^4 - T_2^4), \tag{1}$$

where

q = next flow of radiant heat from black body (or tube) 1 to black body 2,

A_1 = surface area of tube 1,

σ = Stefan-Boltzmann constant,

T_1, T_2 = absolute temperature of 1 and 2,

F_{12} = configuration (or shape) factor between 1 and 2.

Values of configuration factors have been tabulated in the literatures for several shapes,[1] and recently even for parallel cylinders such as the tubes in a fuel bundle.[2] This work presents an equation for calculating the configuration factor between adjacent tubes where no shielding (or shadowing) occurs from other tubes. For closely spaced bundles such as those proposed for most power reactor fuels, a given tube can radiate to four such unshadowed adjacent tubes, four diagonally spaced tubes that are shadowed by the adjacent tubes, and eight more-distant tubes adjacent to the diagonal tubes. Of these 16 tubes receiving direct radiation from the tube, only the four adjacent tubes are not shadowed by other tubes. The calculations of configuration factors becomes considerably more difficult when shadowing occurs, and they defy expression in analytical equations. However, these factors could be evaluated accurately numerically. In the following pages, numerical calculations for the adjacent as well as other tubes are described because the procedures in the latter cases are only modifications of a procedure used for adjacent tubes.

Two assumptions were made to greatly simplify the problem:

1. The tube lengths were considered infinite compared with their radii and spacing.

2. Each tube was considered to have a uniform surface temperature. If this were not true, one would have to approximate the tube by several surfaces assumed to be at a uniform temperature.

Considerable discussion of geometrical definitions, interpretations, and calculations of configuration factors can be found in standard textbooks on heat transfer.[3,4] However, for this report one needs only to note

that the configuration factor for radiation from a differential area dA_1 to an arbitrary cylindrical surface A_2 whose generating line is parallel to dA_1 (see Fig. 6) may be expressed by the relation (see p 19 of ref. 4):

$$F_{(d_1)_2} = \frac{(\sin \phi' - \sin \phi'')}{2} \tag{2}$$

Then if dA_1 is part of the surfaces A_1, the configuration factors for radiation from A_1 to A_2 may be evaluated by integrating $F_{(d1)2}$ over A_1:

$$F_{12} = \frac{1}{A_1} \int_{A_1}^{F} F_{(d_1)_2} \, dA_1. \tag{3}$$

3.2.1 Configuration Factors for Adjacent Tubes

Configuration factors for adjacent tubes can be evaluated by considering surfaces A_1 and A_2 as representing two adjacent tubes with radii r and with their centers separated by a distance a. A cross section of the tubes is shown in Fig. 7. Now consider a differential area dA_1 located at a point A on tube 1. Point A is specified by ψ, the angle of rotation from the plane defined by the center lines of the two tubes. The symbols ϕ'' and ϕ' represent angles measured clockwise from the normal to dA_1, at which surface A_2 "appears" and subsequently "disappears" from view. Since the tubes are assumed to be infinitely long, the differential elements of area may be considered of unit length, and Eq. (3) becomes:

$$\begin{aligned} F_{12} &= \frac{1}{2\pi r} \int_0^{2\pi} \frac{\sin \phi' - \sin \phi''}{2} \, r \, d\psi, \\ &= \frac{1}{4\pi} \int_0^{2\pi} (\sin \phi' - \sin \phi'') \, d\psi. \end{aligned} \tag{4}$$

Also since A_2 cannot be seen from the left side of A_1, and $F_{(d_1)_2}$ is an even function of ψ, Eq. (4) can be simplified to:

$$F_{12} = \frac{1}{2\pi} \int_0^{\pi} (\sin \phi' - \sin \phi'') \, d\psi. \tag{5}$$

UNCLASSIFIED
ORNL-LR-DWG 57774

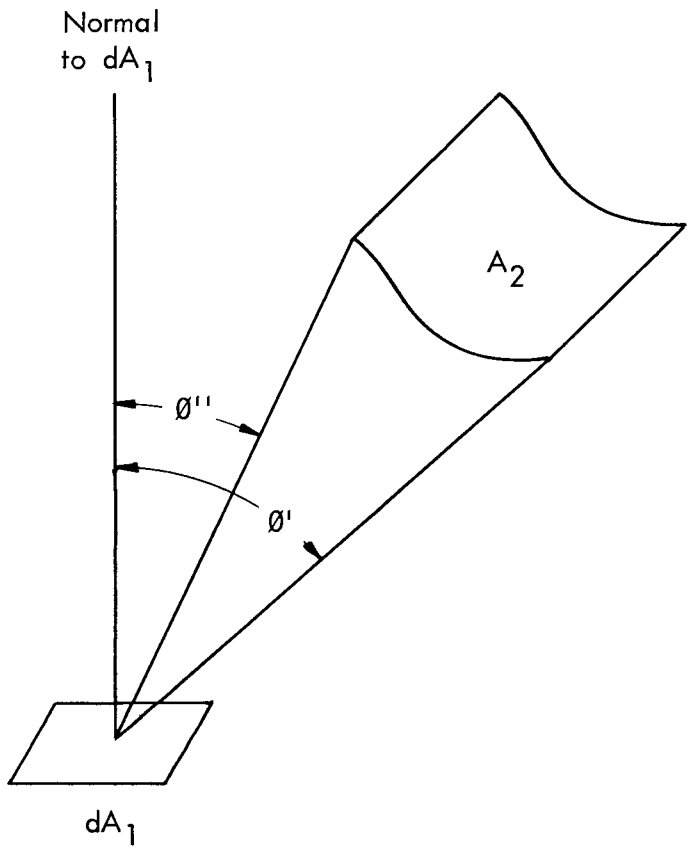

Fig. 6. Geometrical Relationship Between dA_1 and A_2.

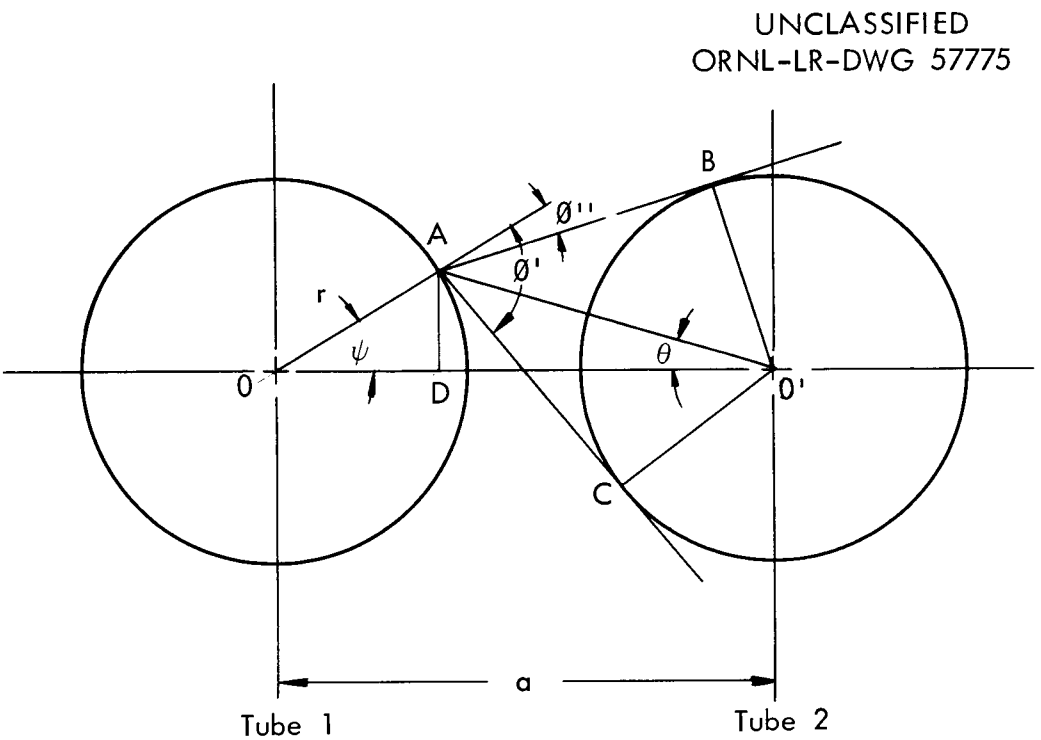

Fig. 7. Cross-Sectional View of Adjacent Tubes, Showing Geometrical Relationships between Parameters Used in Evaluating ϕ' and ϕ''.

To evaluate ϕ' and ϕ'', one must consider the geometry of the system as shown in Fig. 7. Since the triangles OAD and O'AD have the common sides $\overline{AD}$:

$$r \sin \psi = \overline{AO'} \sin \theta. \tag{6}$$

Also, since

$$\overline{OD} + \overline{DO'} = a,$$

it follows that

$$a = r \cos \psi + \overline{AO'} \cos \theta. \tag{7}$$

Solving Eqs. (6) and (7) for θ gives:

$$\theta = \tan^{-1} \frac{r \sin \psi}{[a - (r \cos \psi)]}. \tag{8}$$

By considering the triangle DAO' one can evaluate the length of $\overline{AO'}$:

$$\overline{AO'} = [(r \sin \psi)^2 + (a - r \cos \psi)^2]^{1/2},$$

$$= (a^2 + r^2 - 2ar \cos \psi)^{1/2}. \tag{9}$$

The value of ϕ'' can be calculated by subtracting the angles $\angle$OAD, $\angle$DAO', and $\angle$ O'AB from:

$$\phi'' = \pi - (\frac{\pi}{2} - \psi) - (\frac{\pi}{2} - \theta) - \sin^{-1} (r/\overline{AO'}),$$

$$= \theta + \psi - \sin^{-1} (r/\overline{AO'}). \tag{10}$$

Once ϕ'' is known, ϕ' may be easily calculated by noting that

$$\angle BAO' = \angle CAO'.$$

Therefore,

$$\phi' = \phi'' + 2 \sin^{-1} (r/\overline{AO'}). \tag{11}$$

The above procedure is adequate for calculating ϕ'' and ϕ' for small values of ψ. However, for values of ψ above a critical value, ψ^*, ϕ' calculated in this manner would become greater than $\pi/2$. Since from any point on A_1, A_2 cannot be seen more than $\pi/2$ from the normal, one must substitute $\pi/2$ for ϕ' for all values of ψ above ψ^*. The value of ψ^* can be calculated by noting that at this point $\overline{AO}$ is tangent to the surfaces

of both tube 1 and tube 2. Therefore $\overline{AC}$ intercepts $\overline{OO'}$ midway between the tubes, and

$$\psi^* = \cos^{-1}(2r/a). \tag{12}$$

The above equations can be normalized by making the following substitutions:

$$S = a/r,$$

$$Z = \overline{AO'}/r$$

Then Eqs. (8) through (12) become

$$\Theta = \tan^{-1}\left(\frac{\sin\psi}{S - \cos\psi}\right), \tag{13}$$

$$Z = (S^2 + 1 + 2S\cos\psi)^{1/2}, \tag{14}$$

$$\phi'' = \Theta + \psi - \sin^{-1}(1/Z), \tag{15}$$

$$\phi' = \phi'' + 2\sin^{-1}(1/Z), \tag{16}$$

$$\psi^* = \cos^{-1}(2/S). \tag{17}$$

These relations were used to integrate Eq. (5) numerically with the ORACLE for values of S between 2.0 and 8.0. The results are presented in Table 1 and in Fig. 8. Different sizes of increments were used to check the accuracy of the results, and errors in Table 1 appear to be about 0.05%. The results were also verified by graphically measuring ϕ' and ϕ'' and integrating. The results of the two graphical verifications are shown in Fig. 8. They are within about 5% of the calculated values, which is approximately the accuracy of the graphical measurements.

3.2.2 Configuration Factors for Diagonally Located Tubes

In a square-pitched array, each tube can radiate to tubes located diagonally to the pitch as well as to adjacent tubes. The configuration factor for radiation to a diagonal tube, F_{13}, can be calculated from the relations developed for adjacent tubes provided that a suitable reassignment of variables and tests for "shadowing" by the adjacent tubes are made.

Table 1. Configuration Factors for Adjacent Tubes

S	F_{12}	S	F_{12}
2.00	0.1824	3.00	0.1108
2.05	0.1755	3.10	0.1069
2.10	0.1696	3.20	0.1033
2.15	0.1643	3.30	0.09989
2.20	0.1594	3.40	0.09673
2.25	0.1549	3.50	0.09377
2.30	0.1507	3.60	0.09099
2.35	0.1468	3.70	0.08838
2.40	0.1431	3.80	0.08592
2.45	0.1396	3.90	0.08359
2.50	0.1363	4.00	0.08340
2.55	0.1332	4.25	0.07639
2.60	0.1302	4.50	0.07197
2.65	0.1274	4.75	0.06805
2.70	0.1247	5.00	0.06453
2.75	0.1221	5.50	0.05851
2.80	0.1197	6.00	0.05352
2.85	0.1173	7.00	0.04575
2.90	0.1151	8.00	0.03996
2.95	0.1129	10.00	0.03190
		12.00	0.02655

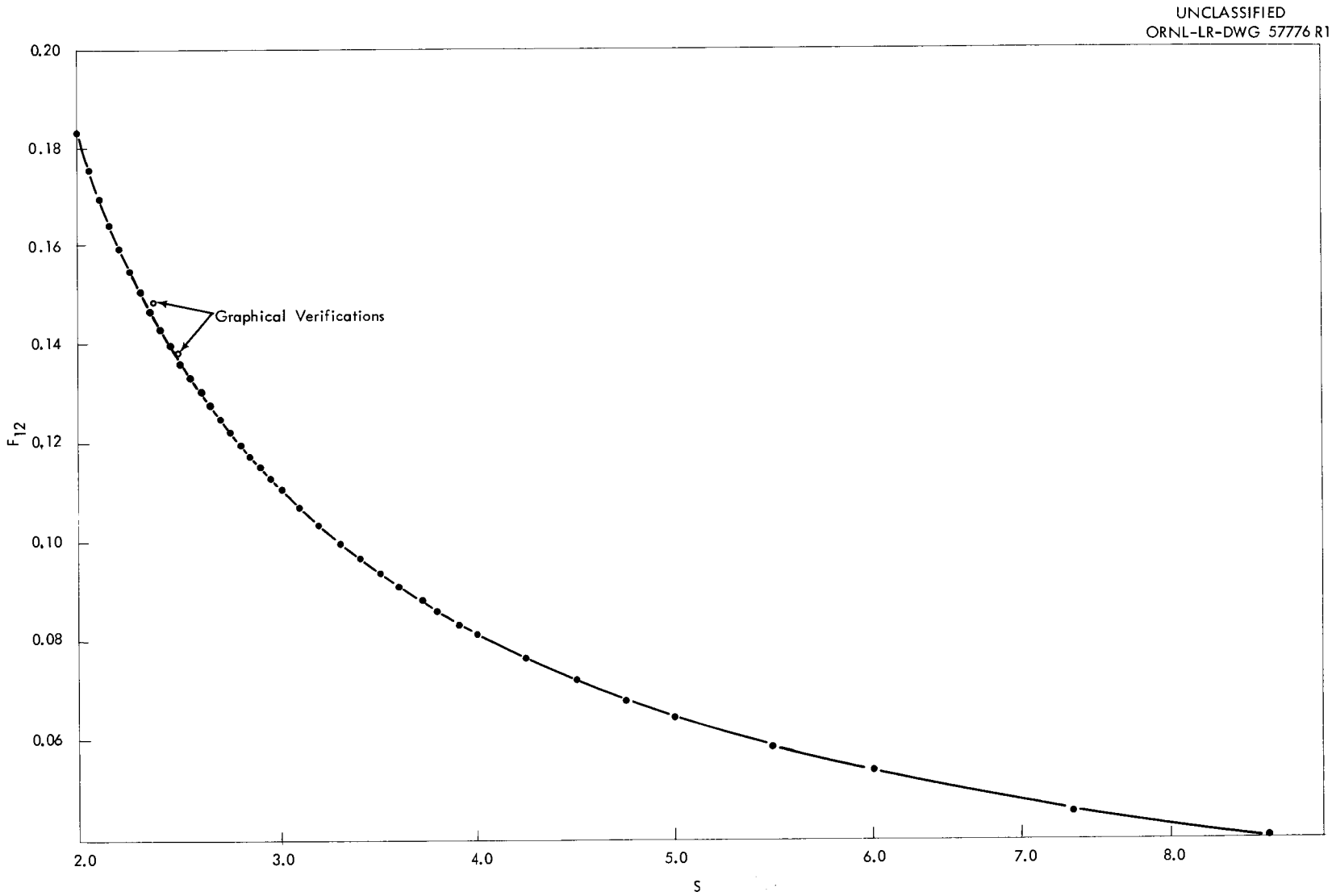

Fig. 8. Numerically-Determined Configuration Factors for Adjacent Tubes.

First it is appropriate to note that for any spacing ratio S greater than $2\sqrt{2}$ there is no shadowing from the adjacent tube. This can be seen with the aid of Fig. 9. Triangle ABO' is a right triangle with $\angle ABO' = \angle AO'B = \pi/4$. Also in normalized distances, AO' = 1 (radius of tube 2) and BO' = S/2.

$$S^* = \frac{2}{\sin \pi/4} = 2\sqrt{2} \quad . \tag{18}$$

Thus for any spacing greater than S^*, the configuration factor can be obtained by letting

$$S' = S\sqrt{2}$$

and finding the factor for S' in Table 1 or Fig. 8. Tubes 1 and 2 are equivalent to two adjacent tubes with spacing S'.

For values of S less than S^*, ϕ'_{13} and ϕ''_{13} may be calculated by using Eqs. (8) through (13) by substituting S' for S and

$$\psi' = \psi - \pi/4$$

for ψ (Fig. 10). Starting at $\psi' = 0$, the integration is identical to that described for adjacent tubes until $\overline{AC}$ intersects tube O'''. This occurs when the condition shown in Fig. 10 occurs. Here,

$$\overline{OF} = S - \overline{FO'''} \quad ;$$

Noting that

$$\angle DO'''O'' = \psi^* = \cos^{-1}(2/S),$$

and that

$$\angle O'''ED = \pi/2 - \psi^*,$$

it is apparent that

$$\overline{OF} = S - S/2 \tan(\pi/2 - \psi^*),$$

$$= S\left(1 - \frac{1}{2 \tan \psi^*}\right).$$

Also, by noting that the line AFDEC has a slope of $\pi/4 - \psi^*$, one can write equations to describe the line and the circle representing tube 1. Solving these equations for the distance FG one finds that

UNCLASSIFIED
ORNL-LR-DWG 57777

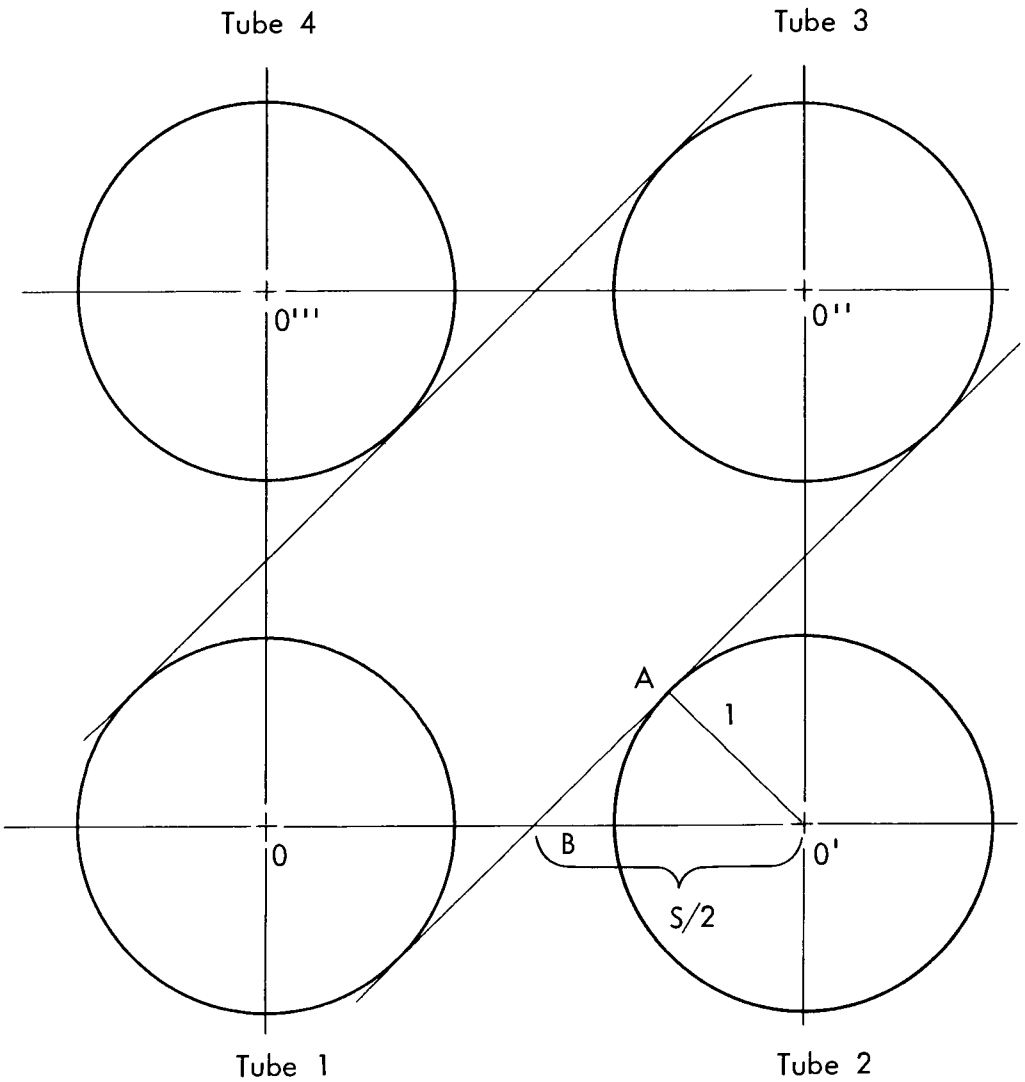

Fig. 9. Cross-Sectional View of Tubes, Showing the "Tightest" Spacing at which Radiation to Diagonal Tubes is not Shadowed by Adjacent Tubes.

UNCLASSIFIED
ORNL-LR-DWG 57778 R1

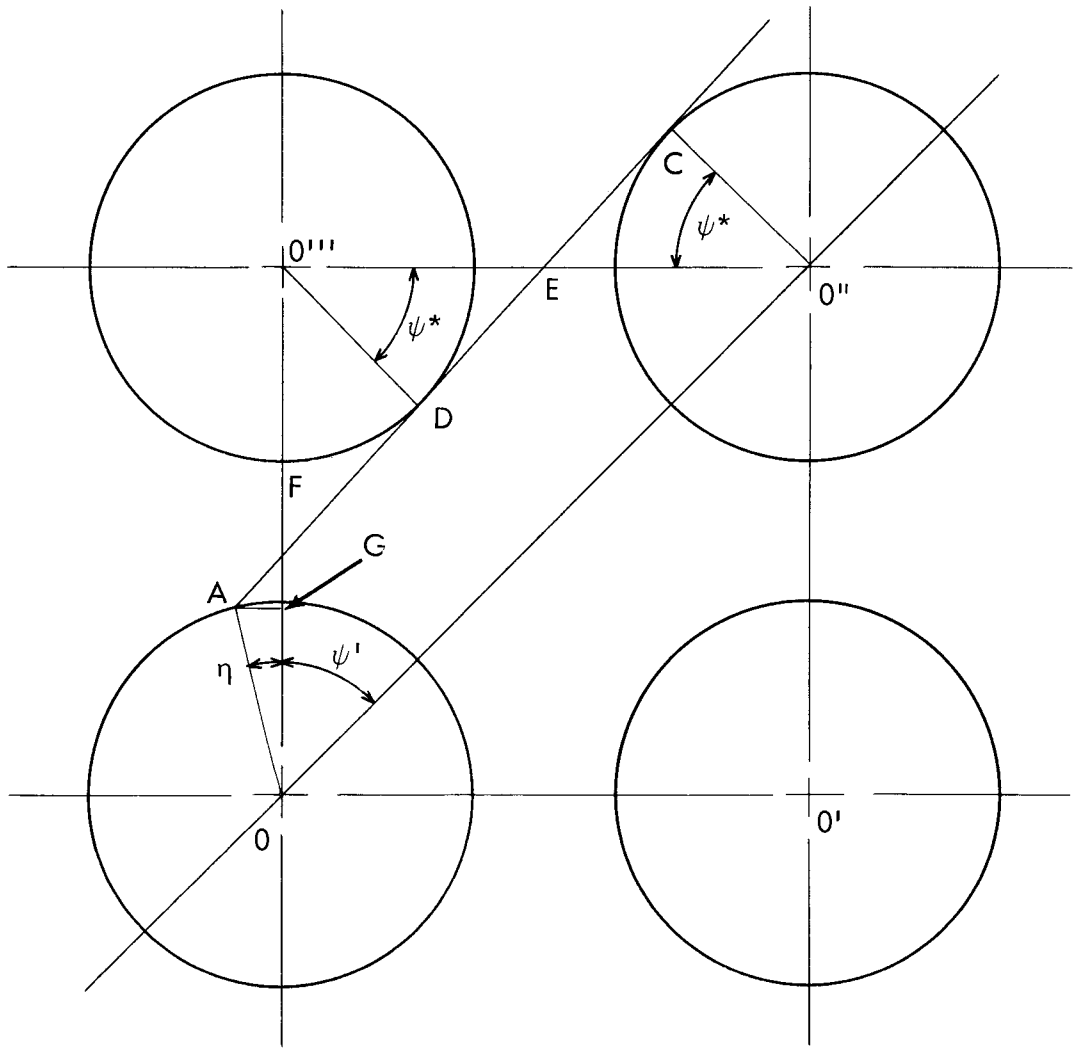

Fig. 10. Cross-Sectional View of Tubes, Showing the Value of ψ' at which Shadowing of the Adjacent Tubes Influence the Numerical Evaluation of the Configuration Factor between Diagonally-Spaced Tubes.

$$\overline{FG} = \frac{\overline{OF} - \sqrt{\overline{OF}^2 - (1 + \tan^2 \psi^*)(\overline{OF}^2 - 1)}}{1 + \tan^2 \psi^*} \quad , \tag{19}$$

Then, from triangle AFG:

$$\eta = \sin^{-1} (\overline{FG} \tan \psi^*), \tag{20}$$

and

$$\bar{\psi} = \eta + \pi/4. \tag{21}$$

For values of ψ' greater than $\bar{\psi}$, ϕ'' must be calculated from the tangent from A to tube 4. This again can be done using Eqs. (8) through (13), provided that one substitutes $\psi' - \pi/4$ for ψ and uses S instead of S'. The value of ϕ' calculated by using these conditions can be substituted for the ϕ'' desired for the integration with respect to ψ'. The integration can be terminated when

$$\psi' = \psi^* + \pi/4.$$

Thus one can calculate the configuration factor for diagonal tubes by using the same equations involved for adjacent tubes, but suitable substitutions for ψ and S are required over each of the regions covered by the integration. These calculations were also performed by the ORACLE, and the results are shown in Table 2 and graphically in Fig. 11. As mentioned before, the calculations were needed only for values of S between 2.0 and $2\sqrt{2}$ since configuration factors for values of S greater than this may be obtained from Fig. 8. Again the calculations were verified graphically, and those results are shown in Fig. 11.

3.2.3 Configuration Factors for Radiation Between Tubes Further Separated in the Array

The tubes in most currently proposed reactor fuel elements have rather tight spacings (low values of S). Consequently, as noted earlier, each tube can radiate to only four adjacent tubes, four diagonal tubes, and eight more-distant tubes located adjacently to the diagonal tubes. If these are the only tubes that can receive radiation from tube 1, then the configuration factor for radiation between tube 1 and each of the eight more-distant tubes may be evaluated by noting that

Table 2. Configuration Factors for Diagonal Tubes

S	F_{13}
2.0000	0.06891
2.0500	0.07402
2.1000	0.07803
2.1500	0.08107
2.2000	0.08337
2.2500	0.08509
2.3000	0.08632
2.3500	0.08714
2.4000	0.08760
2.4500	0.08774
2.5000	0.08760
2.5500	0.08721
2.6000	0.08659
2.6500	0.08577
2.7000	0.08475
2.7500	0.08356
2.8000	0.08221
2.8284	0.08138

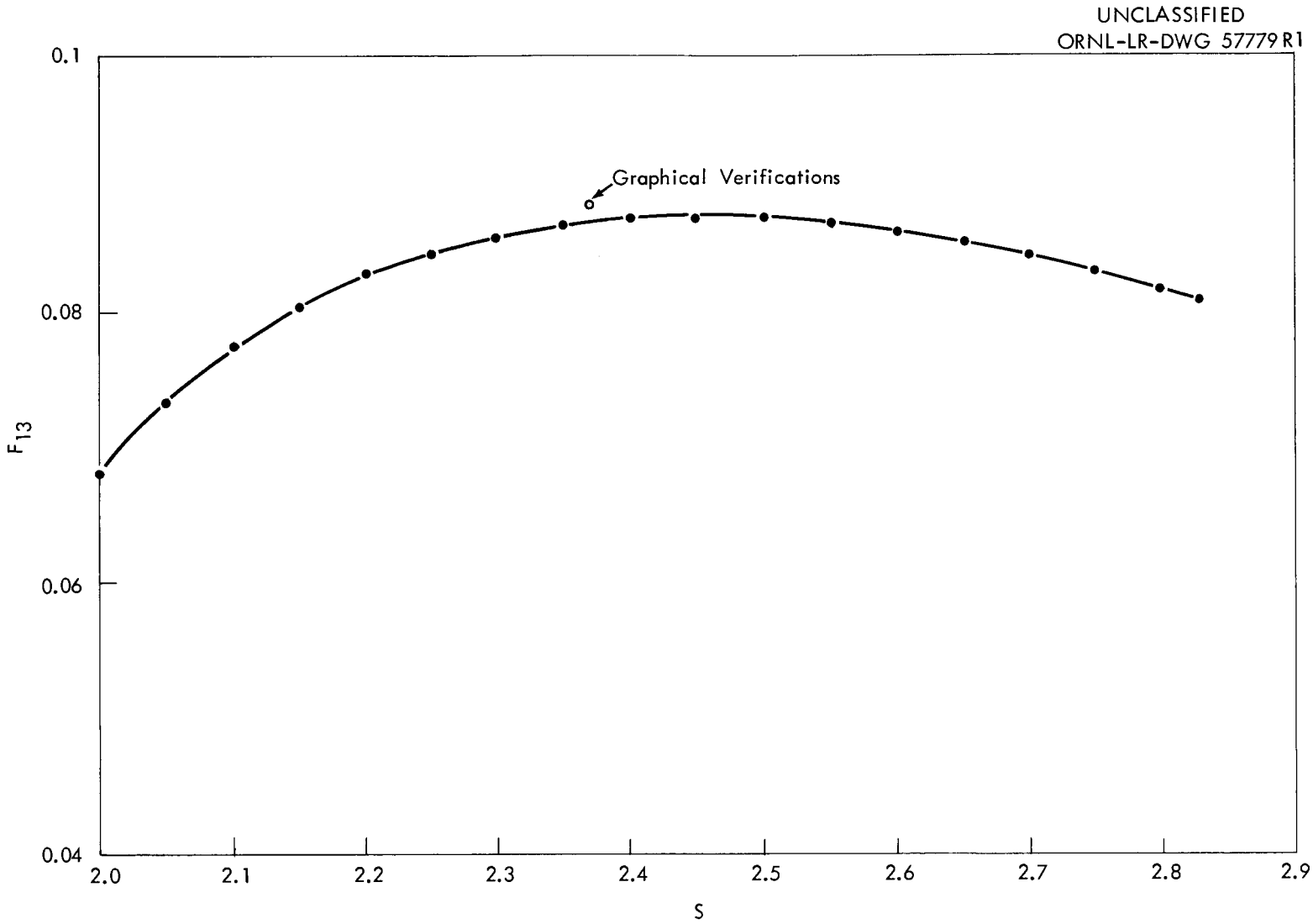

Fig. 11. Numerically-Determined Configuration Factors for Diagonally-Spaced Tubes.

$$\sum_k F_{1k} = 1.$$

Therefore

$$F_{14} = \frac{1 - 4(F_{12} + F_{13})}{8}, \tag{22}$$

where

F_{12} = configuration factor between adjacent tubes,

F_{13} = configuration factor between diagonally located tubes, and

F_{14} = configuration factor between further-separated tubes.

If the spacing S is large enough that more tubes may receive radiation from the first tube, then calculations of configuration factors become more difficult. It then will probably become necessary in such cases to obtain less exact results graphically.

3.3 Estimation of Grey-Body Radiation Factors

Although Eq. (1) may be used to calculate the net radiant fluxes within a system of black bodies, the problem becomes much more complicated for grey bodies because all the thermal energy incident upon a surface is not absorbed; a substantial fraction may be reflected. In general, the net radiant flux from a surface 1 to a surface 2 is calculated from relations of the form:

$$Q_{12} = A_2 \, \mathcal{F}_{12} \, \sigma(T_1^4 - T_2^4) \ , \tag{23}$$

where $\mathcal{F}_{12}$ is the grey-body radiation factor between 1 and 2. The term $\mathcal{F}_{12}$ represents a complicated function of areas, emissivities, and configuration factors not only for radiation between surfaces 1 and 2 but between all surfaces in the system. Accordingly, $\mathcal{F}_{12}$ must account for all the heat from tube 1 which reaches tube 2 through complicated multiple reflections from surrounding tubes as well as by direct radiation.

Some consideration was given to evaluations of $\mathcal{F}$'s in the manner described by McAdams and credited to Hottel, but, for the many surfaces involved in this problem, the correct evaluation of the $\mathcal{F}$'s appeared to be too unwieldly to be practical. Even if these calculations had been made,

it appears that the results would have had to be simplified considerably before the temperatures in tube bundles could have been predicted. Actually $\mathcal{F}_{ij}$ is not simply a function of the relative positions of tubes i and j (adjacent, diagonal, etc.), but it is also a function of the absolute position of these tubes in the array (except probably for tubes near the center of very large arrays). Furthermore, $\mathcal{F}_{ij}$ will be a function of the size of the array (number and location of reflecting surfaces). It appeared likely that a substantial simplification of the true problem was needed, such as assuming that $\mathcal{F}_{ij}$ is a function of only the relative position of i and j and is independent of the size of the bundle. Thus a semiempirical method (discussed below) of evaluating $\mathcal{F}_{ij}$ under these assumptions appeared most promising.

Although several methods of estimating $\mathcal{F}_{ij}$ were tried, the following system appeared to give the most satisfactory results, although it leaves much to be desired, especially for small bundles. The surfaces i and j were the only surfaces giving off or receiving heat (obviously, an incorrect but useful assumption); all other surfaces were assumed to be no-flux surfaces, and all surfaces were assumed to have the same emissivity. Accordingly, the grey-body radiation factor becomes:[4]

$$\mathcal{F}_{ij} = \frac{1}{\frac{1}{\overline{F}_{ij}} + 2\left(\frac{1}{\epsilon} - 1\right)} , \tag{24}$$

where ϵ is the emissivity of all surfaces. The term $\overline{F}_{ij}$ is defined by the relation:

$$\overline{F}_{ij} = F_{ij} + F_{iR} \frac{F_{Rj}}{1 - F_{RR}} , \tag{25}$$

where R represents the no-flux surfaces surrounding i and j. Equation (23) was used to evaluate the radiant flux between the various tubes in the array. To keep the values of $\mathcal{F}_{ij}$ reasonably conservative, $\overline{F}_{ij}$ was taken equal to F_{ij}. This essentially neglected any heat going to j from R.

3.4 Predictions of the Temperature Distributions within Fuel Bundles: A Proposed Method

Once values have been obtained for the radiation factors ($\mathcal{F}$'s), one can predict the temperature distribution if all heat were transferred by radiation governed by these coefficients. All the heat generated within a given tube must be radiated to all other tubes that can receive its radiation. Then the net heat radiated, Q_i, from tube i will be:

$$Q_i = A\sigma \sum_{j=1}^{N} \mathcal{F}_{ij}(T_i^{\,4} - T_j^{\,4}). \tag{26}$$

An expression such as this can be written for each tube in the bundle, and these equations (linear in T^4) can be solved simultaneously for each T^4. For large tube bundles of varying size, a rapidly converging trial-and-error procedure appeared to be simpler for solving these equations than setting up and evaluating the determinates for direct solution.

Equation (26) can be solved for $T_i^{\,4}$ to give:

$$T_i^{\,4} = \frac{\dfrac{Q_i}{A} + \sum\limits_{j=1}^{N} \mathcal{F}_{ij} T_j^{\,4}}{\sum\limits_{j=1}^{N} \mathcal{F}_{ij}}. \tag{27}$$

For tubes well inside the bundle, N=16, because each internal tube "sees" 16 other surrounding tubes. For tubes on the side of the bundle but not on the corner, N=10, because these tubes see nine other tubes and the wall of the cask. For corner tubes, N=6, because these see five other tubes and the wall of the cask. Tubes just one row inside the bundle, or next to the outside of the bundle, radiate to 14 tubes and to the wall.

In the trial-and-error procedure adopted for predicting temperature distributions, the temperature of all tubes were initially set at the temperature of the wall of the cask. Then the temperature required for each tube to radiate its generated heat was calculated from Eq. (27) and assigned to that tube. The calculations were repeated throughout the bundle until the temperature of the center tube changes less than 0.01°C

in repeated calculations. As noted earlier, Eq. (27) appears somewhat different for corner tubes of the bundle, for outside tubes, for tubes one row from the outside, and for tubes further inside the bundle because of differences in N. It would have been desirable to write a simple code that simply iterated through the bundle, solving Eq. (27). However, it appeared necessary to consider the outside and corner tubes as special cases and to use Eq. (27) separately for these. However, the tubes just one row inside the bundle transfer very little heat directly to the wall, and a special treatment seemed unnecessary. These tubes were heated just as the inner tubes were, but, to approximate the small amount of heat transferred to the wall, an additional row of tubes was imagined to be placed around the bundle in order to simulate the wall for these tubes.

A considerable reduction in computation could be obtained by noting that the temperatures within the bundle were symmetrical. One needs only evaluate the temperatures in about one octant of the bundle. Accordingly, this approach was coded in FORTRAN and compiled on an IBM-7090 computer. The results were compared with the experimental data and gave reasonable predictions of the measured temperature distributions, as will be seen in a later section of this report. The source program is shown in Appendix A, and a deck of the source or object code can be obtained from the author.

4. RESULTS

Temperature distributions were measured in fuel bundles containing from 16 to 64 tubes, and the results are shown in Figs. 13 through 40; shells simulating casks with internal cavities 6 and 12 in. in diameter were used. In some cases, the temperature distribution was determined with the cask in horizontal and vertical positions.

Although the recommended method for estimating the temperature distribution is based solely upon radiation, significant convection was very clearly shown in the data. For example, when the cask and fuel bundles were in the horizontal position, the temperature distribution was not symmetrical about a horizontal plane through the center of the fuel element. The tubes in the upper portion of the element were significantly hotter than those in the corresponding positions in the lower portion of the array.

Also, the wall temperature was not uniform, as can be seen in Fig. 12. The higher wall temperatures at the top of the cask are expected to result from the convective chimney above the heated element. However, remember that an actual cask with heavy lead walls should be expected to conduct heat in the angular direction better than these simulated casks and consequently should show less angular dependence of wall temperature.

There were also indications that radiation was important. This was noted especially with the larger bundles and smaller casks where one would expect convection to be more difficult; the maximum temperatures were located relatively close to the center of the bundle. This could be conceived to result also from convection, but this behavior is considered more of an indication of radiation (or possibly conduction). The strongest argument for the importance of radiation, however, still hinges on the relatively high temperatures obtained and one's ability to estimate roughly the temperatures obtained by radiation-based calculations.

The largest fuel bundles studied contained 64 tubes in an 8 x 8 array. The 5/16-in. tubes were spaced with 0.37 in. between centers. This is essentially the tube size and spacing of the Consolidated Edison fuel. The temperature distributions in the bundle are shown in Figs. 13 through 23. Figures 13 through 17 show results obtained with the cask in the horizontal position. Along with the experimental results, the calculated temperature distribution is shown, using the suggested calculation procedure. The experimental and estimated results are reasonably close for the highest heat generation rates where the temperatures are above 200°C. However, just as expected, at lower temperatures, radiation is not so important, and the estimated temperatures are considerably above those measured experimentally.

Figures 18 through 23 show results obtained with the cask and fuel bundle in the vertical position. Here, the measured and predicted temperature distributions are both symmetrical. Again, the measured and estimated temperatures are very close when the heat generation rate is high, but the agreement is poor at low heat generation rates and low temperatures. Figures 21 through 23 show the temperature distribution measured when the thermocouples were withdrawn slightly from the midpoint of the bundle

UNCLASSIFIED
ORNL-LR-DWG 62886

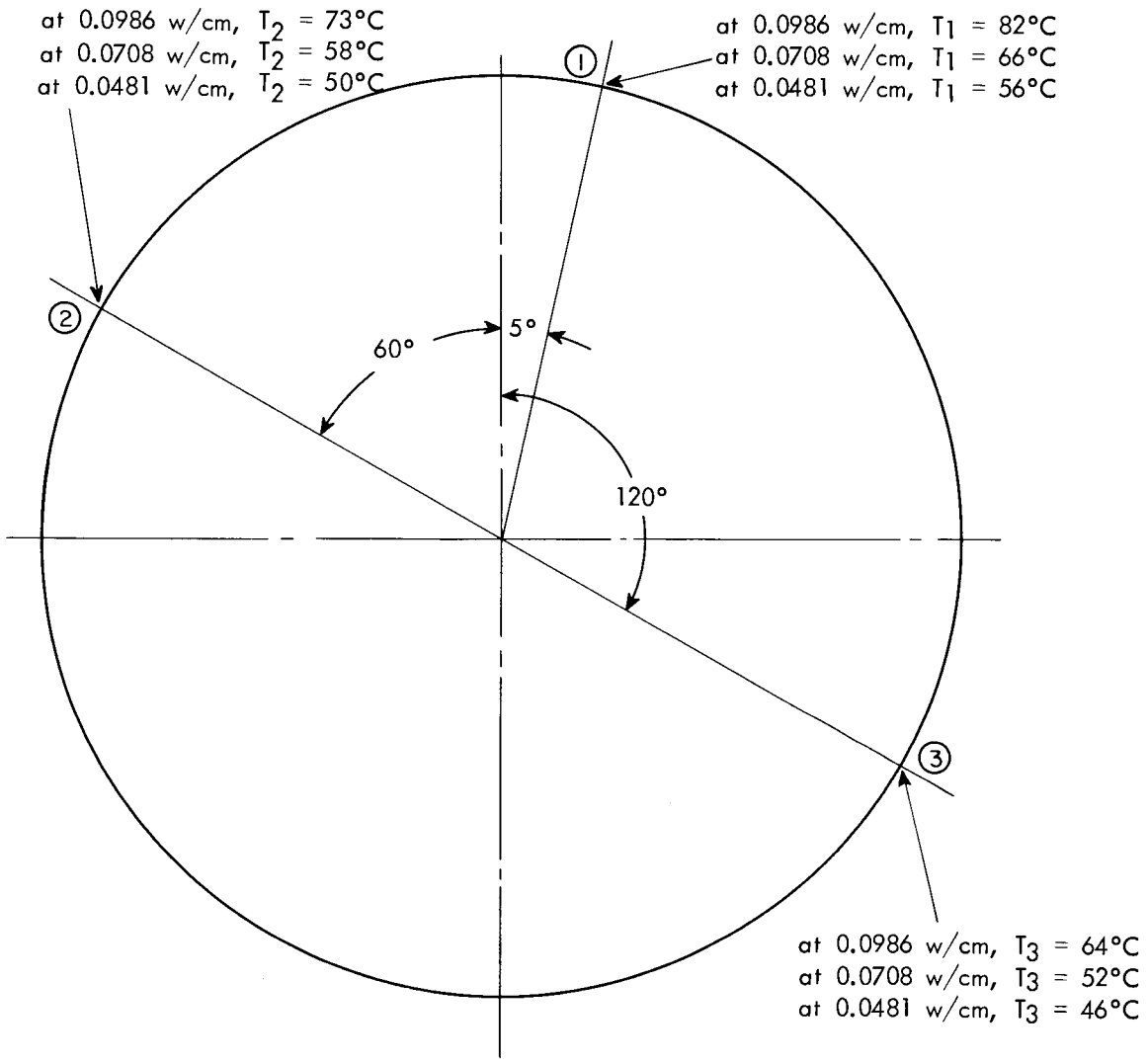

Fig. 12. Dependence of the Temperature of the Wall of the Cask on Angular Position.

UNCLASSIFIED
ORNL-LR-DWG. 78730

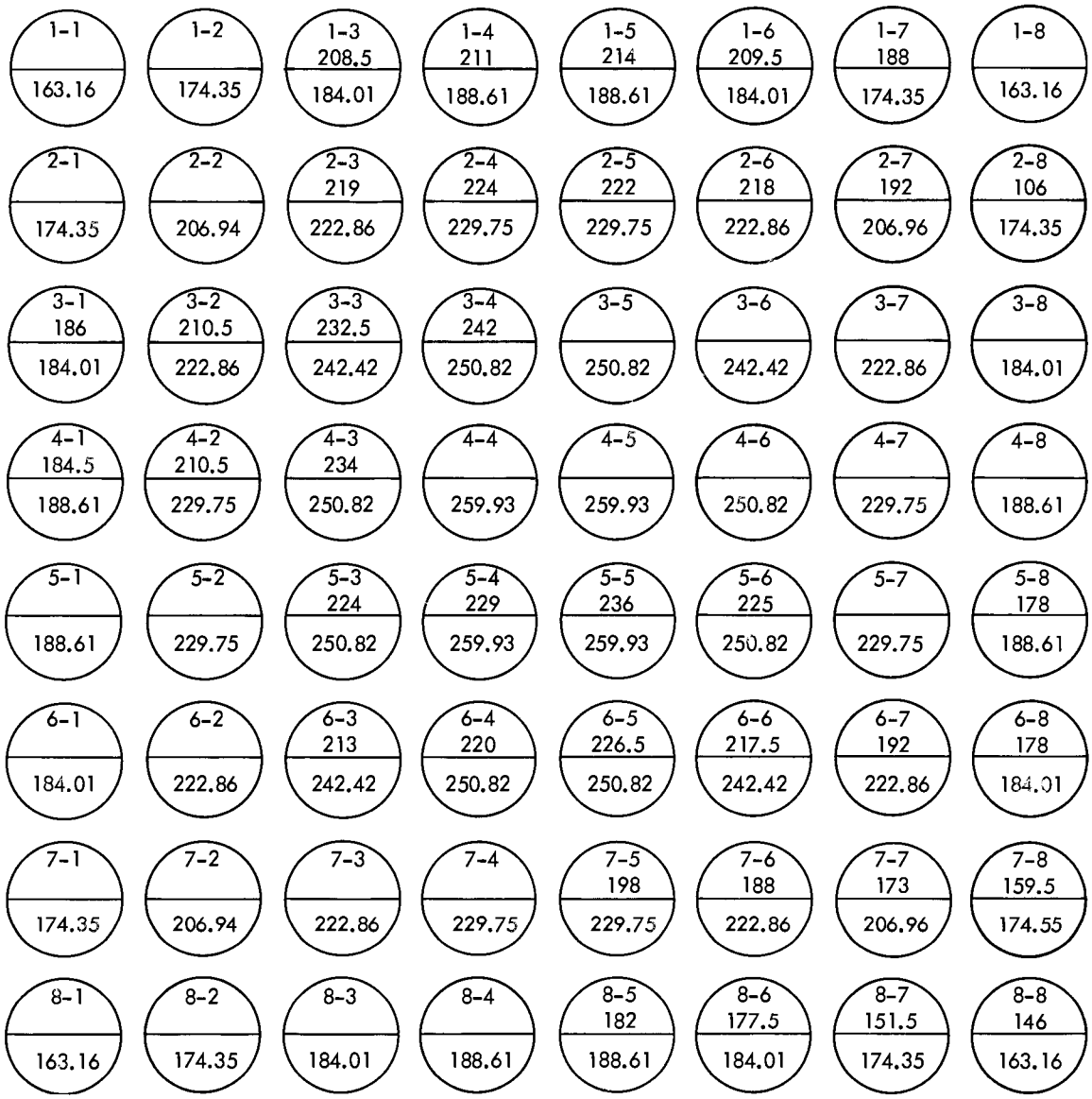

Fig. 13. Predicted and Experimental Temperature Distribution in a 64-Tube Bundle, Square Array, Horizontal Position. Predicted temperatures (°C) are shown in the lower half of the circles. Q = 0.0514 w/cm of tube; average wall temperature = 79.0°C.

UNCLASSIFIED
ORNL-LR-DWG. 78731

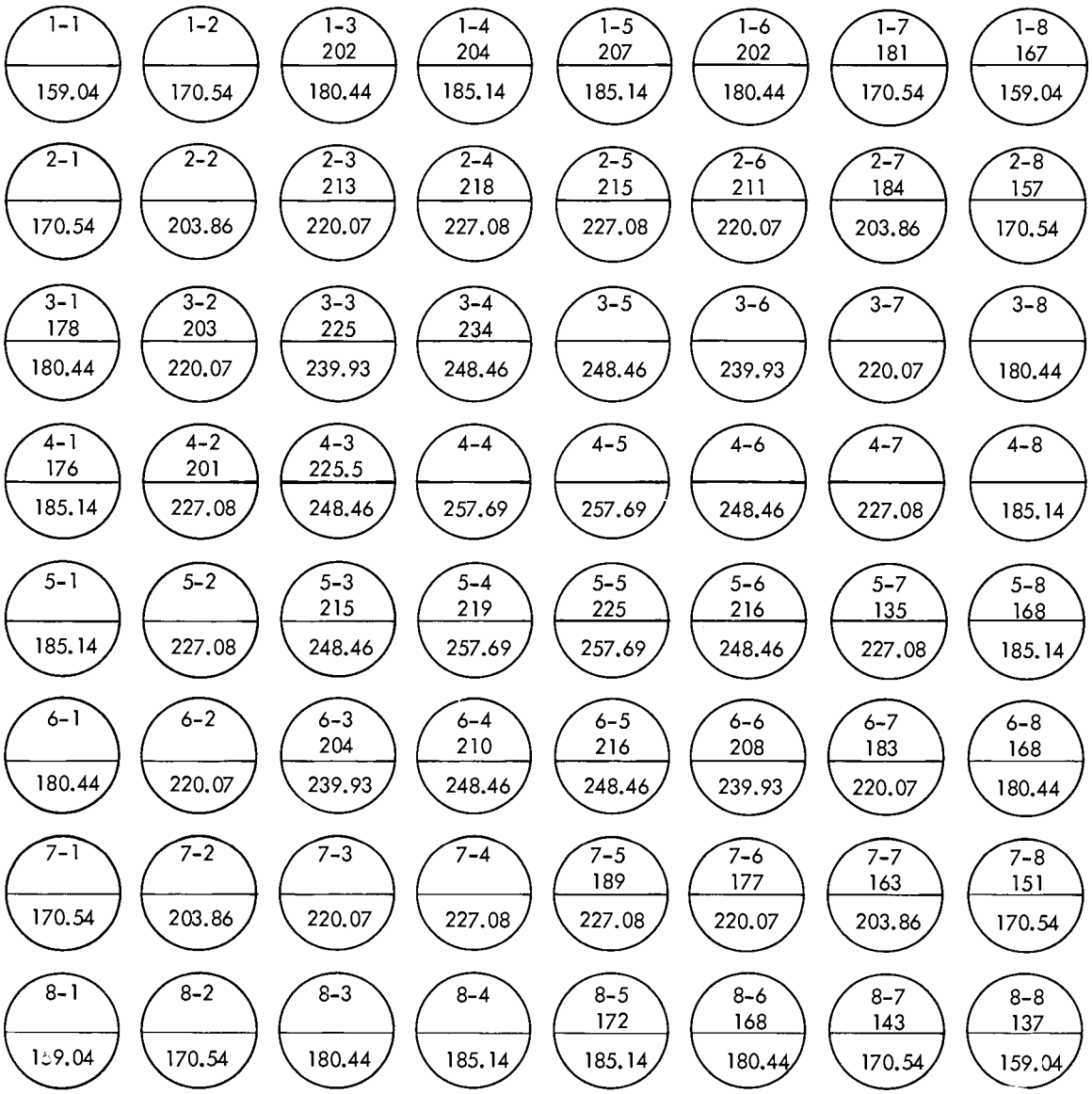

Fig. 14. Predicted and Experimental Temperature Distribution in a 64-Tube Bundle, Square Array, Horizontal Position. Predicted Temperatures (°C) are shown in the lower half of the circles. Q = 0.0514 w/cm of tube; average wall temperature = 71.0°C.

UNCLASSIFIED
ORNL-LR-DWG. 78732

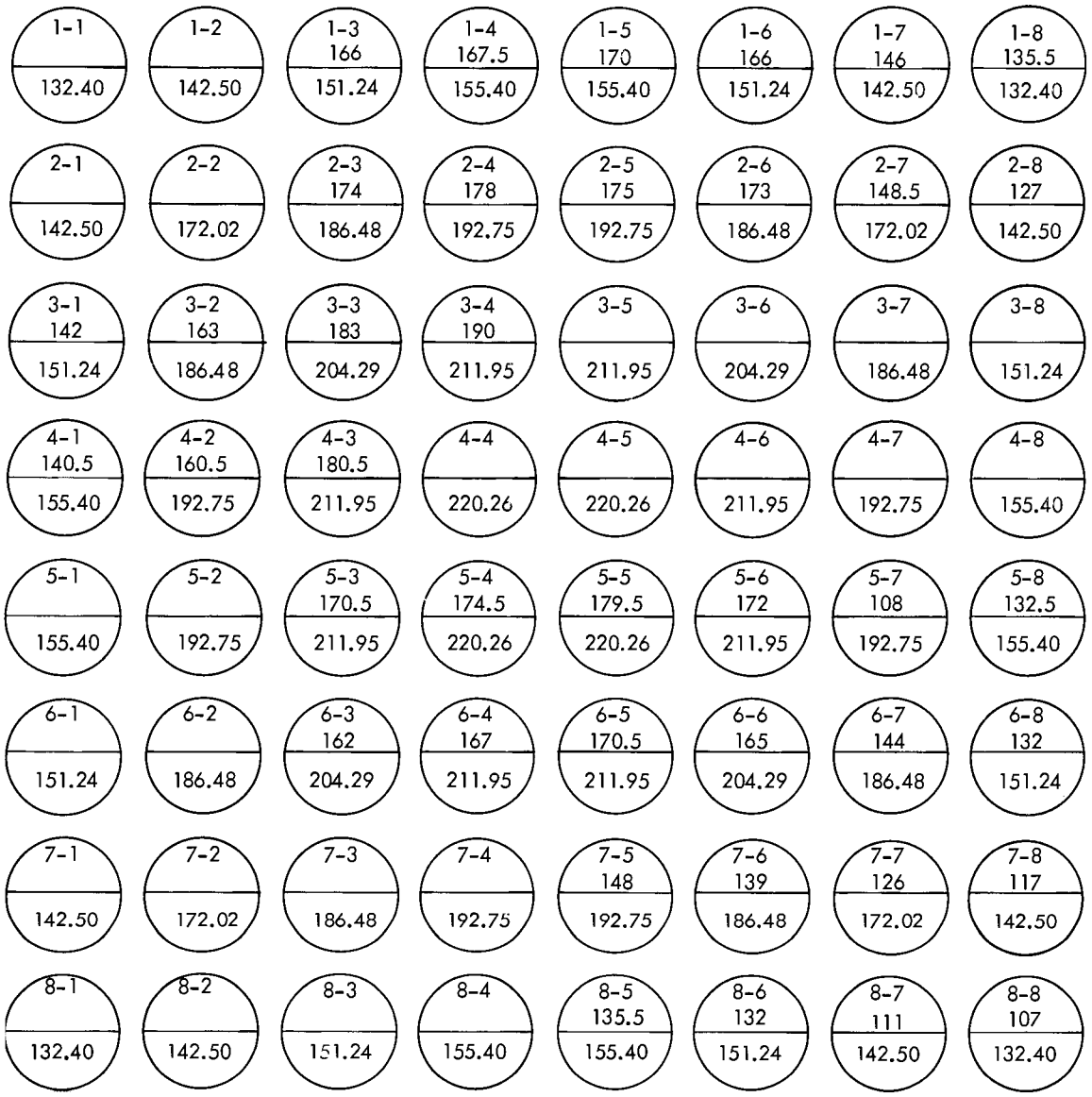

Fig. 15. Predicted and Experimental Temperature Distribution in a 64-Tube Bundle, Square Array, Horizontal Position. Predicted temperatures (°C) are shown in the lower half of the circles. Q = 0.0372 w/cm of tube; average wall temperature = 57.5°C.

UNCLASSIFIED
ORNL-LR-DWG. 78733

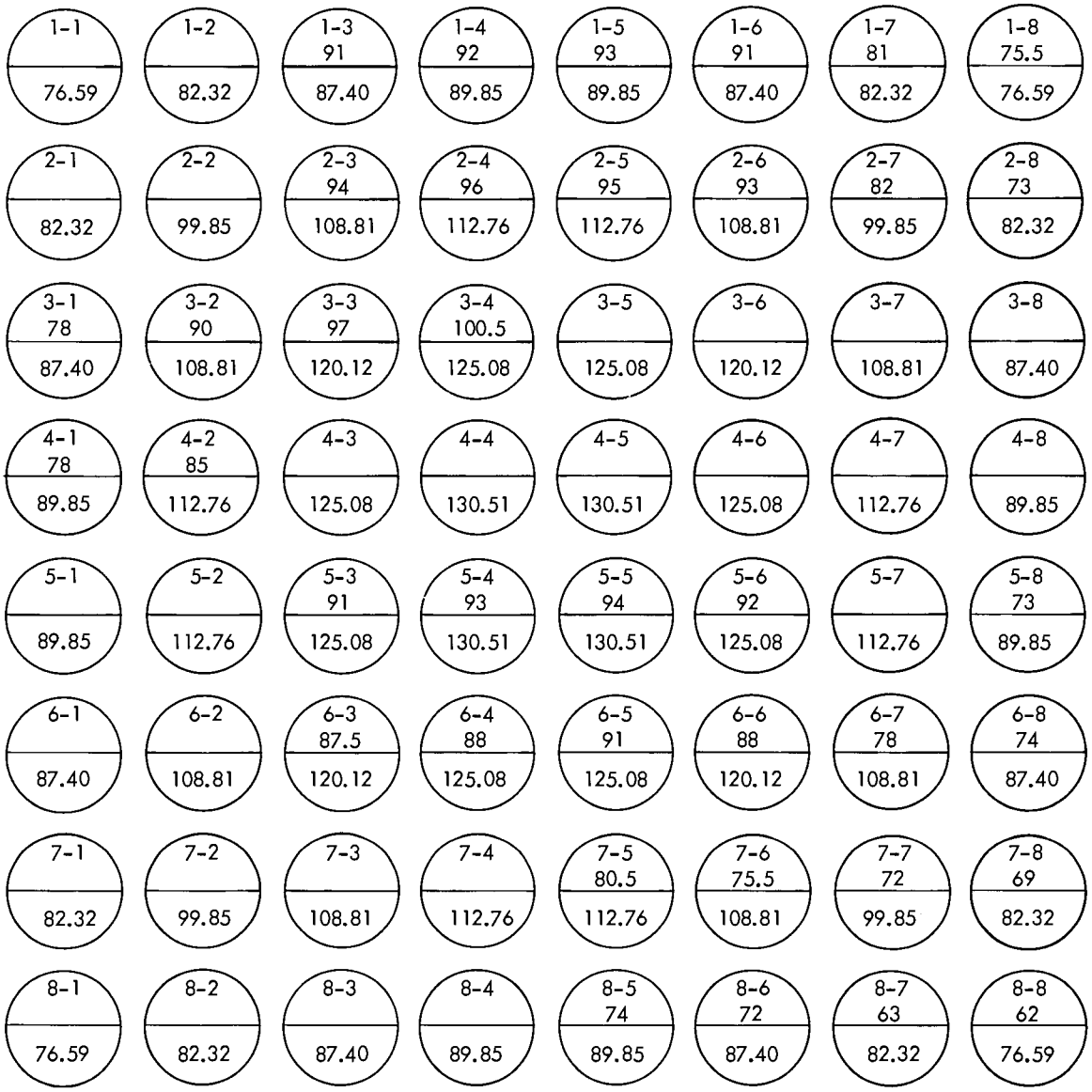

Fig. 16. Predicted and Experimental Temperature Distribution in a 64-Tube Bundle, Square Array, Horizontal Position. Predicted Temperatures (°C) are shown in the lower half of the circles. Q = 0.01338 w/cm of tube; average wall temperature = 39.3°C.

UNCLASSIFIED
ORNL-LR-DWG. 78734

1-1 / 55.93	1-2 / 58.90	1-3 56 / 61.58	1-4 56.5 / 62.89	1-5 57 / 62.89	1-6 56 / 61.58	1-7 52.5 / 58.90	1-8 51 / 55.93
2-1 / 58.90	2-2 / 68.37	2-3 59 / 73.42	2-4 58 / 75.69	2-5 57 / 75.69	2-6 57 / 73.42	2-7 53.5 / 68.37	2-8 48 / 58.90
3-1 51.5 / 61.58	3-2 56 / 73.42	3-3 59 / 79.99	3-4 61 / 82.93	3-5 / 82.93	3-6 / 79.99	3-7 / 73.42	3-8 / 61.58
4-1 51.5 / 62.89	4-2 54.5 / 75.69	4-3 60.5 / 82.93	4-4 / 86.19	4-5 / 86.19	4-6 / 82.93	4-7 / 75.69	4-8 / 62.89
5-1 / 62.89	5-2 / 75.69	5-3 57 / 82.93	5-4 59.5 / 86.19	5-5 58 / 86.19	5-6 58 / 82.93	5-7 / 75.69	5-8 48 / 62.89
6-1 / 61.58	6-2 / 73.42	6-3 57 / 79.99	6-4 56 / 82.93	6-5 57 / 82.93	6-6 55.5 / 79.99	6-7 51 / 73.42	6-8 49 / 61.58
7-1 / 58.90	7-2 / 68.37	7-3 / 73.42	7-4 / 75.69	7-5 52 / 75.69	7-6 51 / 73.42	7-7 48 / 68.37	7-8 46 / 58.90
8-1 / 55.93	8-2 / 58.90	8-3 / 61.58	8-4 / 62.89	8-5 50 / 62.89	8-6 49 / 61.58	8-7 44.5 / 58.90	8-8 44 / 55.93

Fig. 17. Predicted and Experimental Temperature Distribution in a 64-Tube Bundle, Square Array, Horizontal Position. Predicted temperatures (°C) are shown in the lower half of the circles. Q = 0.005712 w/cm of tube; average wall temperature = 38.3°C.

UNCLASSIFIED
ORNL-LR-DWG. 78735

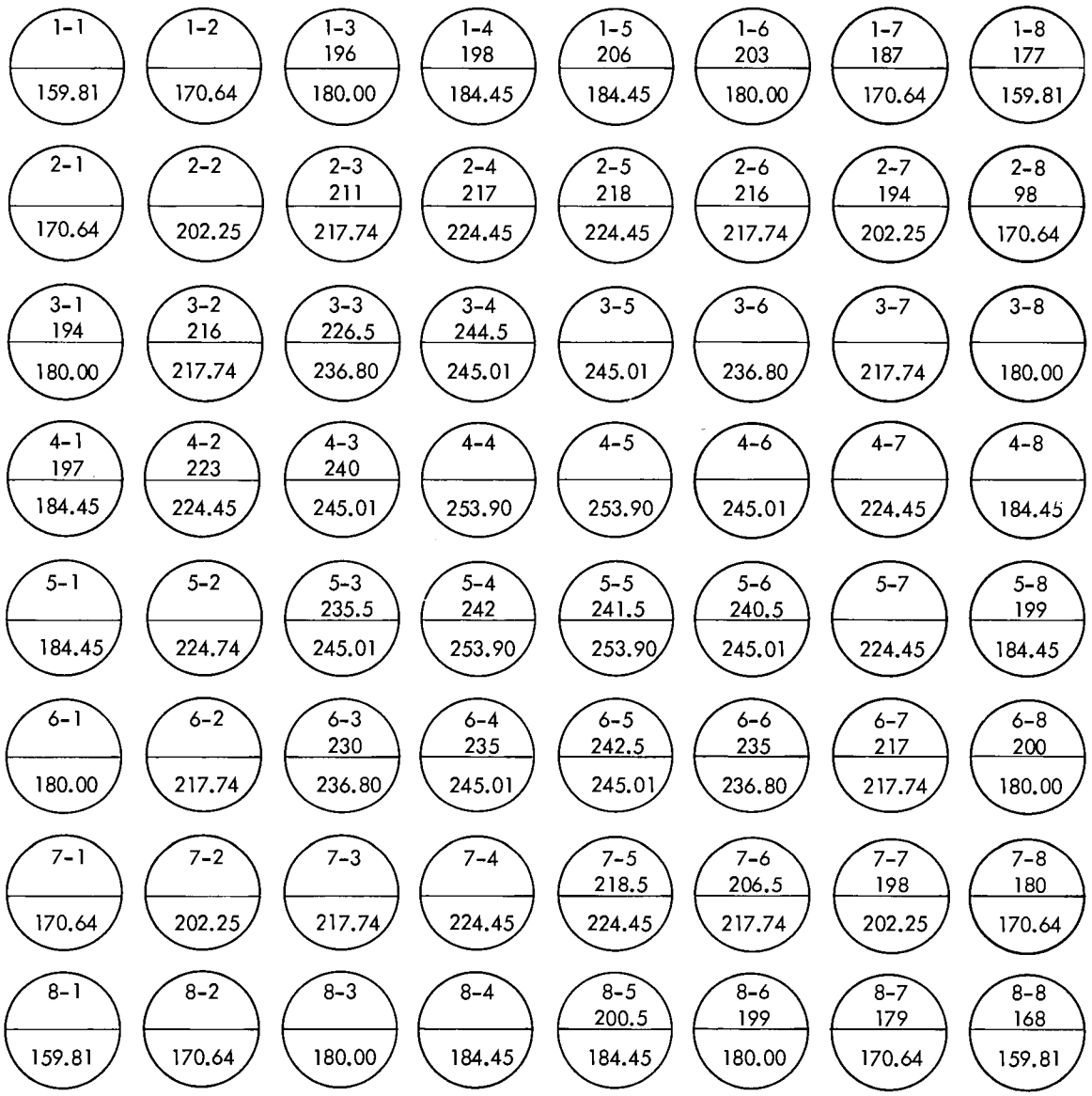

Fig. 18. Predicted and Experimental Temperature Distribution in a 64-Tube Vertical Bundle at the Midpoint. Predicted temperatures (°C) are shown in the lower half of the circles. Q = 0.04852 w/cm of tube; average wall temperature = 79.4°C.

UNCLASSIFIED
ORNL-LR-DWG. 78736

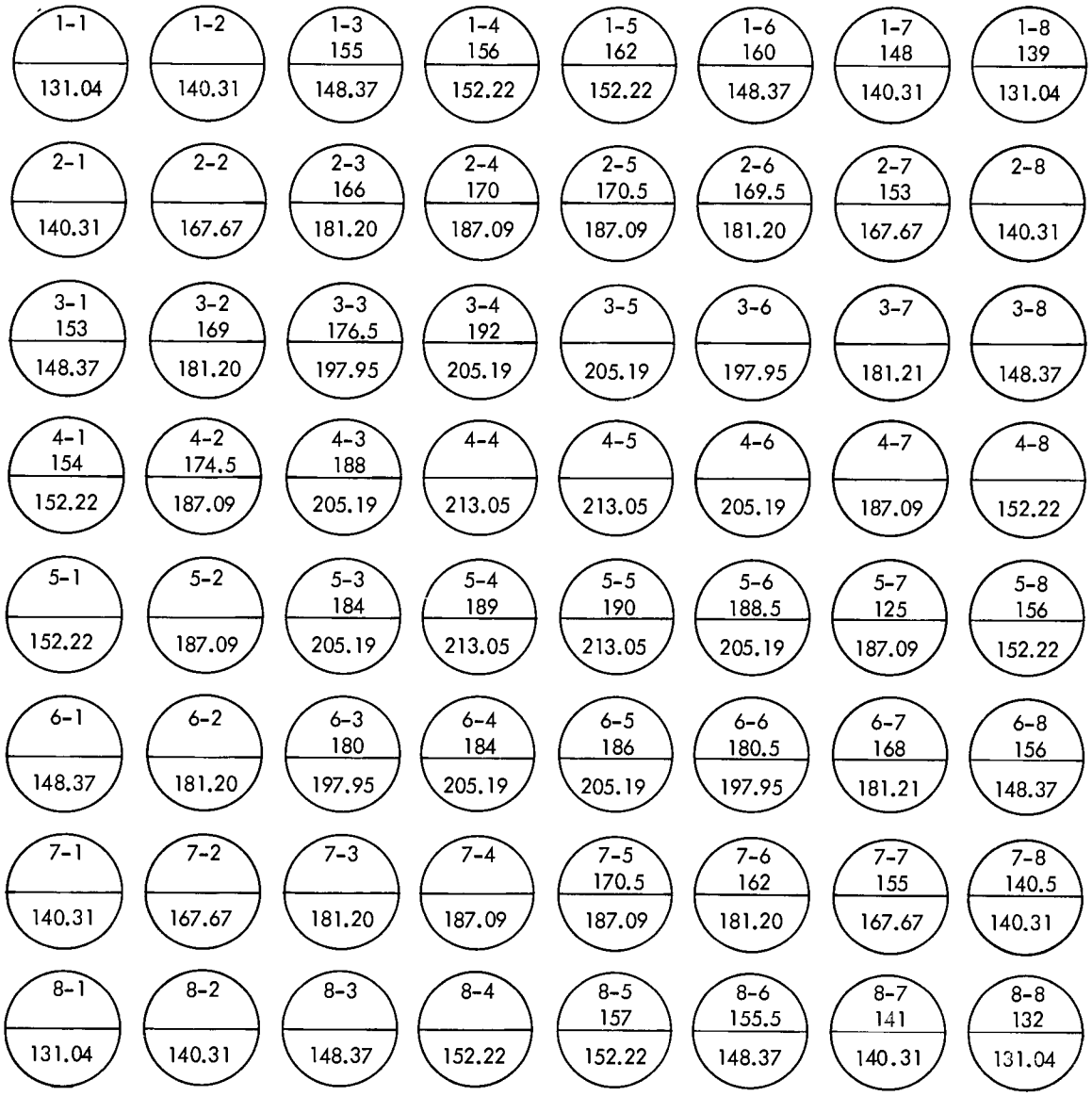

Fig. 19. Predicted and Experimental Temperature Distribution in a 64-Tube Vertical Bundle at the Midpoint. Predicted temperatures (°C) are shown in the lower half of the circles. Q = 0.0337 w/cm of tube; average wall temperature = 64.6°C.

UNCLASSIFIED
ORNL-LR-DWG. 78737

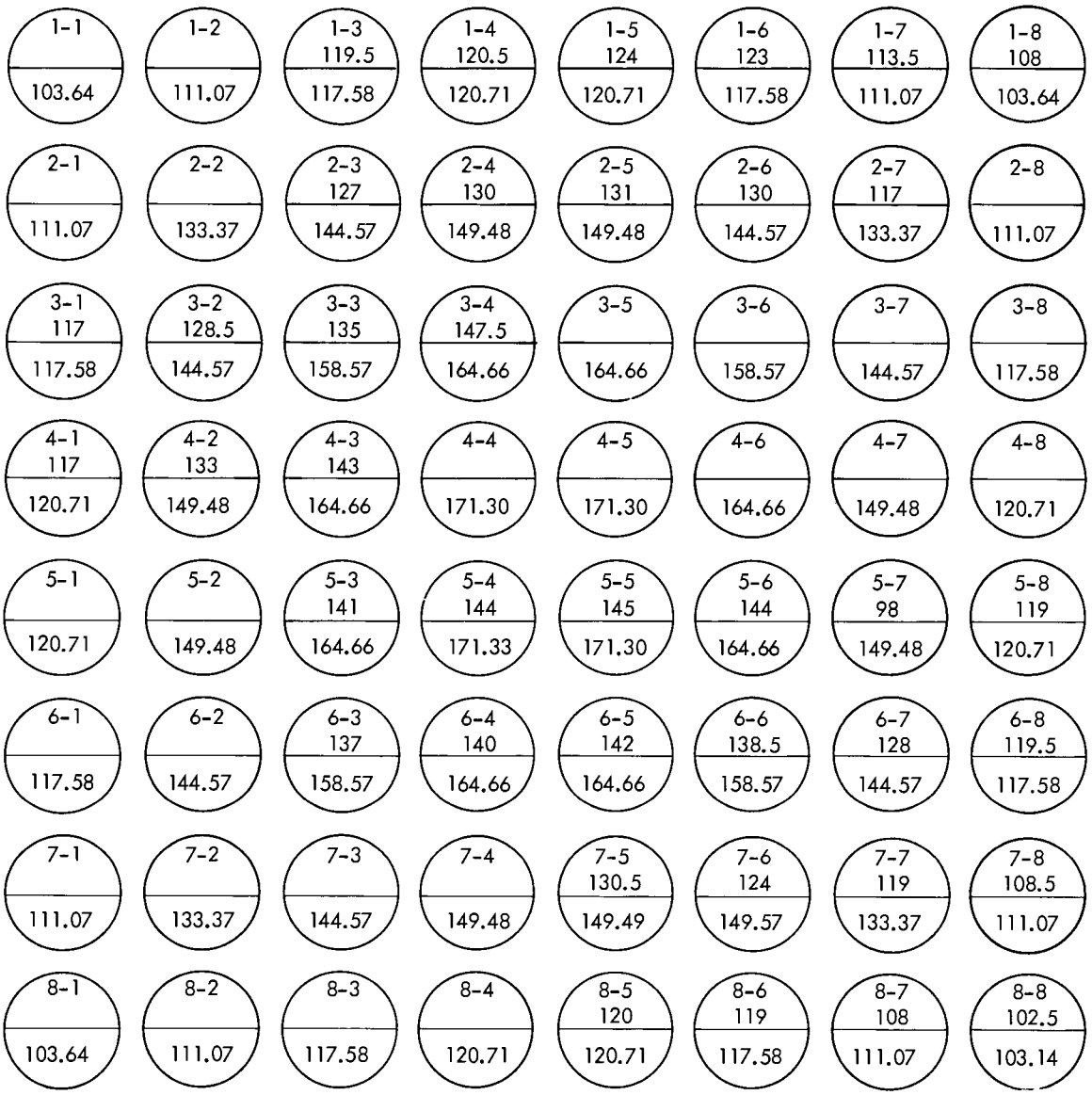

Fig. 20. Predicted and Experimental Temperature Distribution in a 64-Tube Vertical Bundle at the Midpoint. Predicted temperatures (°C) are shown in the lower half of the circles. Q = 0.02158 w/cm of tube; average wall temperature = 53.0°C.

UNCLASSIFIED
ORNL-LR-DWG. 78738

1-1 / 74.95	1-2 / 80.23	1-3 84 / 84.92	1-4 86 / 87.19	1-5 88 / 87.19	1-6 86.5 / 84.92	1-7 80.5 / 80.23	1-8 77 / 74.95
2-1 / 80.23	2-2 / 96.47	2-3 89 / 104.83	2-4 91 / 108.53	2-5 92 / 108.53	2-6 91.5 / 104.83	2-7 82.5 / 96.47	2-8 52.5 / 80.23
3-1 83 / 84.92	3-2 90 / 104.83	3-3 94 / 115.43	3-4 102.5 / 120.09	3-5 / 120.09	3-6 / 115.43	3-7 / 104.83	3-8 / 84.92
4-1 83 / 87.19	4-2 93 / 108.53	4-3 99.5 / 120.09	4-4 / 125.21	4-5 / 125.21	4-6 / 120.09	4-7 / 108.53	4-8 / 87.19
5-1 / 87.19	5-2 / 108.53	5-3 98 / 120.09	5-4 100.5 / 125.21	5-5 101 / 125.21	5-6 100 / 120.09	5-7 71 / 108.53	5-8 85 / 87.19
6-1 / 84.92	6-2 / 104.83	6-3 96.5 / 115.43	6-4 98 / 120.09	6-5 99 / 120.09	6-6 96.5 / 115.43	6-7 90 / 104.83	6-8 85 / 84.92
7-1 / 80.23	7-2 / 96.47	7-3 / 104.83	7-4 / 108.53	7-5 92 / 108.53	7-6 87 / 104.83	7-7 85 / 96.47	7-8 78 / 80.23
8-1 / 74.95	8-2 / 80.23	8-3 / 84.92	8-4 / 87.19	8-5 85 / 87.19	8-6 85 / 84.92	8-7 78 / 80.23	8-8 74.5 / 74.95

Fig. 21. Predicted and Experimental Temperature Distribution in a 64-Tube Vertical Bundle at the Midpoint. Predicted temperatures (°C) are shown in the lower half of the circles. Q = 0.01212 w/cm of tube; average wall temperature = 41.2°C.

UNCLASSIFIED
ORNL-LR-DWG. 78739

1-1 72.17	1-2 77.58	1-3 79.5 82.37	1-4 82 84.68	1-5 83 84.68	1-6 82 82.37	1-7 77.5 77.58	1-8 72 72.17
2-1 77.58	2-2 94.16	2-3 89.5 102.66	2-4 91 106.42	2-5 91 106.42	2-6 90.5 102.66	2-7 84 94.16	2-8 50 77.58
3-1 79 82.37	3-2 92.5 102.66	3-3 96 113.44	3-4 99.5 118.17	3-5 118.17	3-6 113.44	3-7 102.66	3-8 82.37
4-1 80.5 84.68	4-2 94.5 106.42	4-3 100.5 118.17	4-4 101.5 123.36	4-5 123.36	4-6 118.17	4-7 106.42	4-8 84.68
5-1 84.68	5-2 106.42	5-3 100.5 118.17	5-4 101 123.36	5-5 101.5 123.36	5-6 98 118.17	5-7 91 106.42	5-8 80.5 84.68
6-1 82.37	6-2 102.66	6-3 97 113.44	6-4 99 118.17	6-5 100 118.17	6-6 98 113.44	6-7 90 102.66	6-8 81 82.37
7-1 77.58	7-2 94.16	7-3 102.66	7-4 106.42	7-5 90.5 106.42	7-6 89.5 102.66	7-7 87 94.16	7-8 77 77.58
8-1 72.17	8-2 77.58	8-3 82.37	8-4 84.68	8-5 80 84.68	8-6 81.5 82.37	8-7 78 77.58	8-8 71.5 72.17

Fig. 22. Predicted and Experimental Temperature Distribution in a 64-Tube Vertical Bundle 15 in. from the Bottom. Predicted temperatures (°C) are shown in the lower half of the circles. Q = 0.01212 w/cm of tube; average wall temperature = 37.4°C.

UNCLASSIFIED
ORNL-LR-DWG. 78740

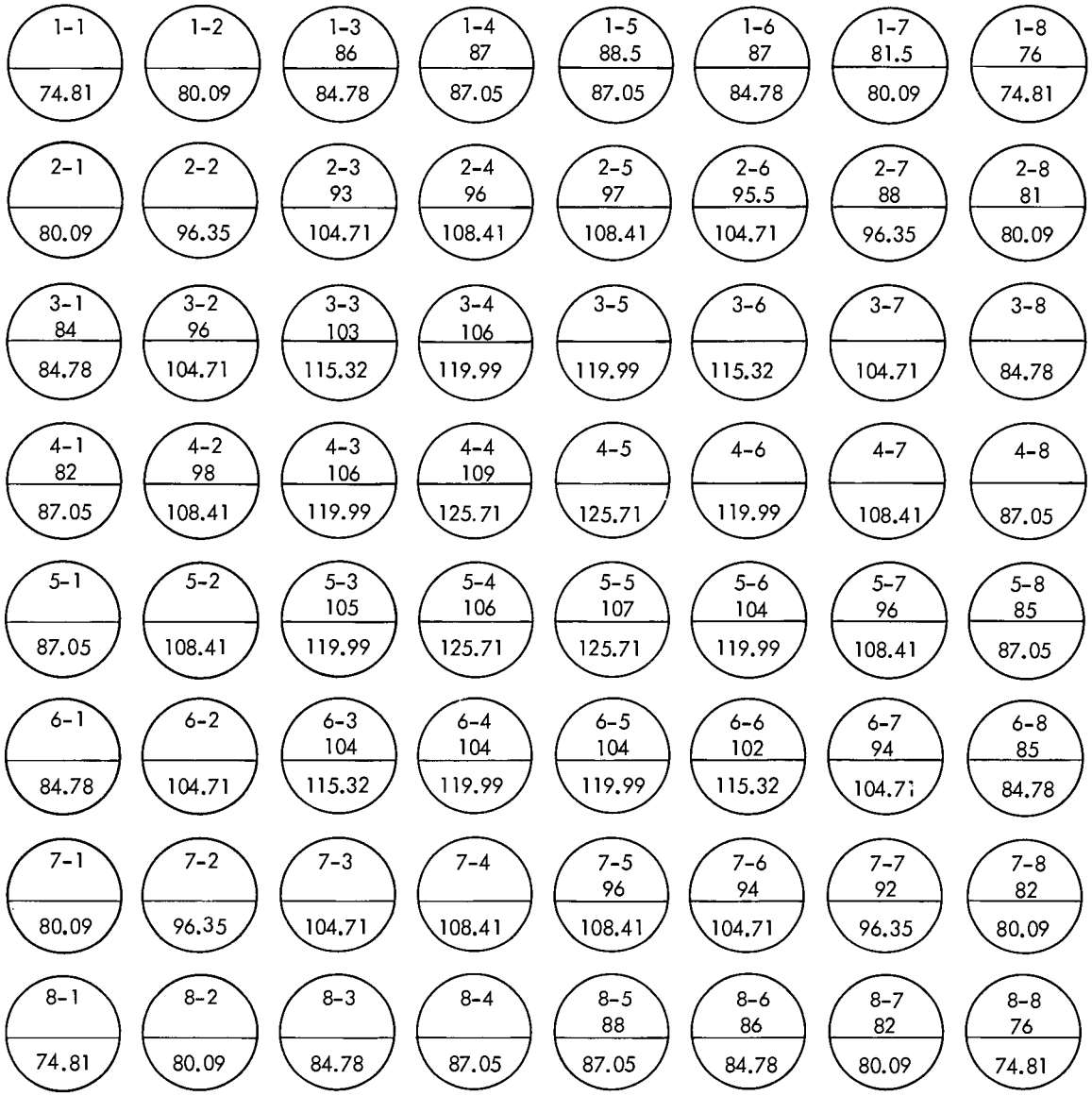

Fig. 23. Predicted and Experimental Temperature Distribution in a 64-Tube Vertical Bundle 18 in. from the Bottom. Predicted temperatures (°C) are shown in the lower half of the circles. Q = 0.01212 w/cm of tube; average wall temperature = 41.0°C.

(12 in. from the bottom of a 24-in.-long bundle). The effects of convection can be seen because there is a slight increase in temperature with height. (Temperature variations not far removed from the center of the horizontal bundle were negligible.)

The use of a smaller fuel bundle in a 12 in. cask gives more space for convection, and, as might be expected, this results in lower temperatures than those estimated by the suggested procedure. It also results in a shift of the hottest tube further from the center of the bundle (with the cask in the horizontal position). Figure 24 shows that in one run a maximum temperature of 248°C was measured one row from the top of a 6 x 6 array, while the maximum temperature estimated in the center of the array was 267°C. As expected, and shown in Figs. 24 through 27, this difference becomes greater as the heat generation rate decreases.

In a similar manner, the results of a 4 x 4 array in the 12 in. cask show even more marked effects of convection, as can be seen in Figs. 28 through 33. Here the maximum temperatures are at the very top of the bundle; therefore the estimated temperatures made by using the suggested procedure are almost useless. These conditions are out of the useful range of the suggested calculational procedure.

However, when a 4 x 4 bundle of tubes was placed in a 6-in. cask, there was much less free space, and one would expect the effects of convection to be much less. As can be seen from Figs. 34 through 40, the measured temperatures are again closer to those estimated. Actually in these cases, the measured temperatures were often slightly higher than the predicted temperatures. This may be partly due to the fact that the measured temperatures are probably a little higher than the surface temperatures (see Sec 2.2), but this does indicate that there are shortcomings in the approximate radiation analysis used in the calculations. It appears likely that the procedure is slightly conservative for calculating the temperature differences from tube to tube, but slightly optimistic with respect to the temperatures of the outer tubes.

UNCLASSIFIED
ORNL-LR-DWG. 78741

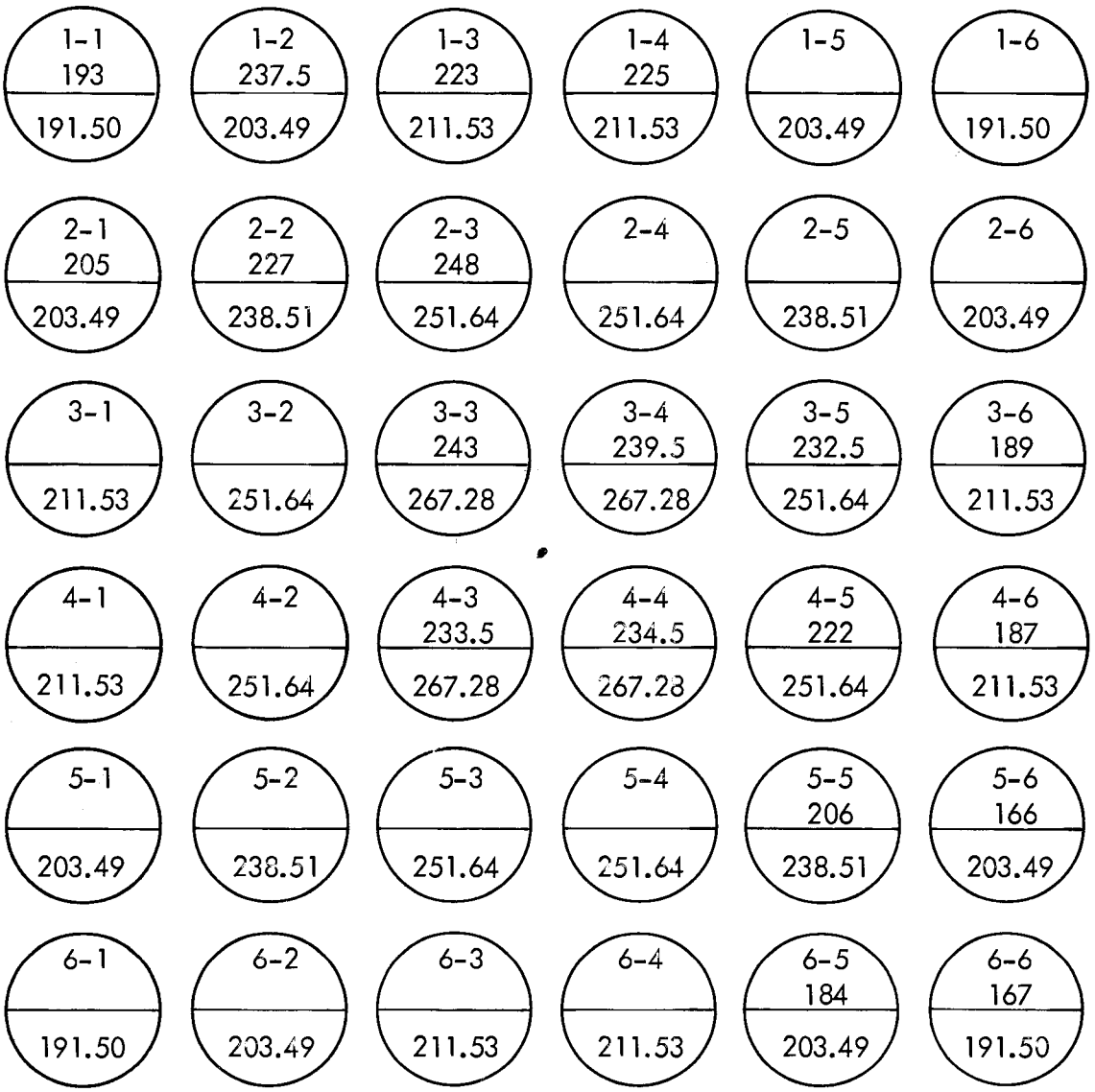

Fig. 24. Predicted and Experimental Temperature Distribution in a 36-Tube Bundle, Square Array, Horizontal Position. Predicted temperatures (°C) are shown in the lower half of the circles. Q = 0.0888 w/cm of tube; average wall temperature = 73.2°C.

UNCLASSIFIED
ORNL-LR-DWG. 78742

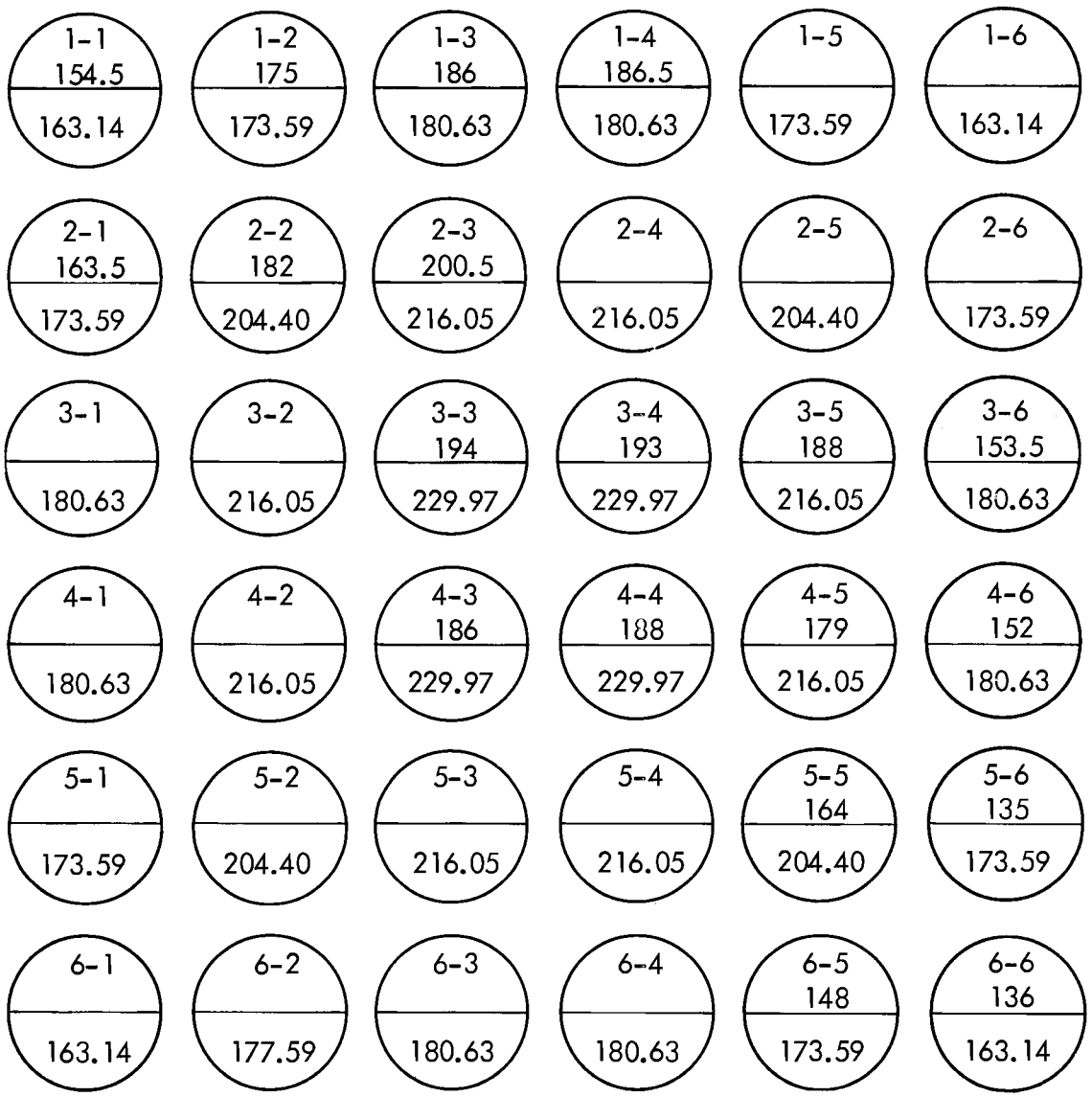

Fig. 25. Predicted and Experimental Temperature Distribution in a 36-Tube Bundle, Square Array, Horizontal Position. Predicted temperatures (°C) are shown in the lower half of the circles. Q = 0.0639 w/cm of tube; average wall temperature = 64.8°C.

UNCLASSIFIED
ORNL-LR-DWG. 78743

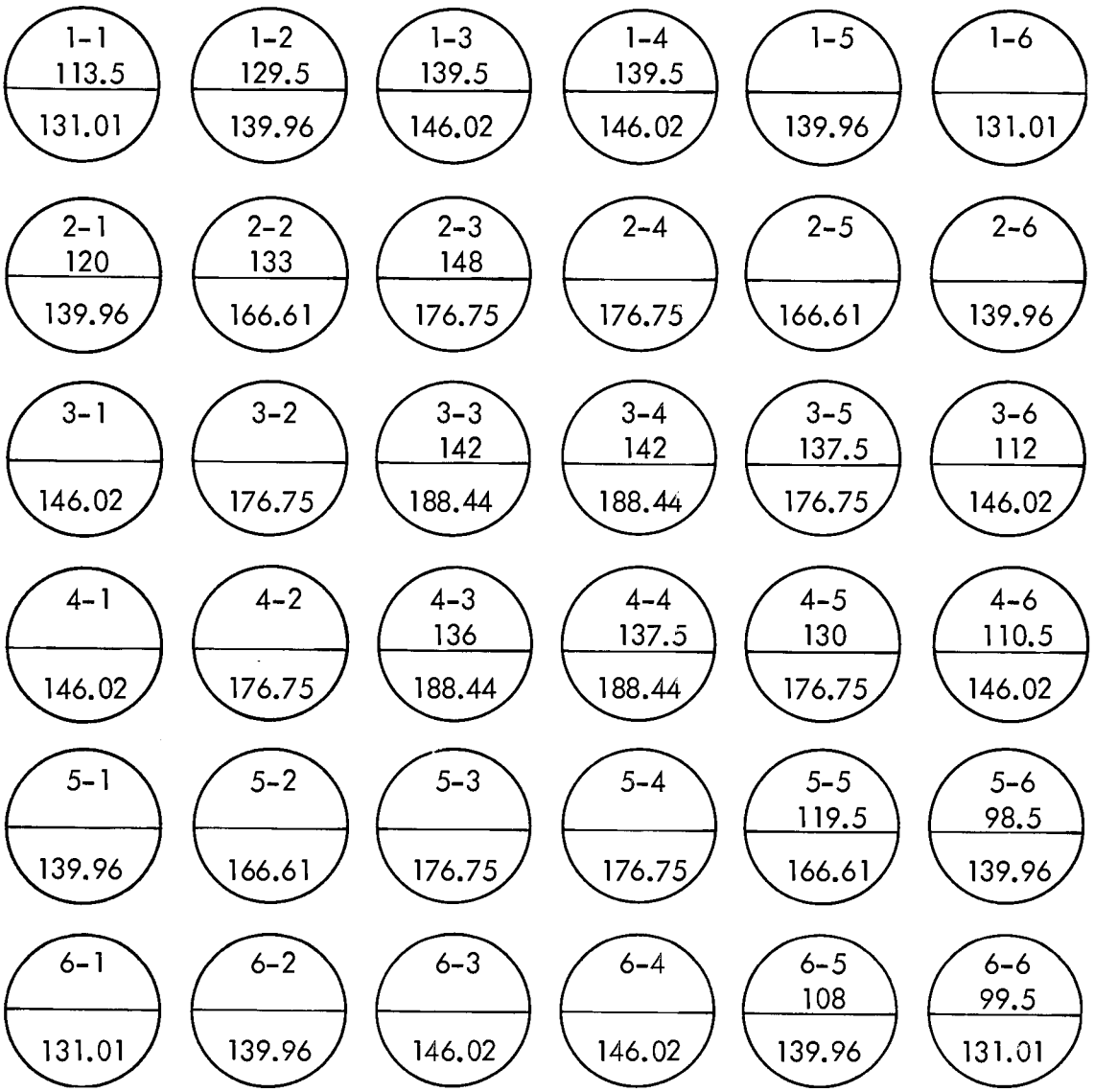

Fig. 26. Predicted and Experimental Temperature Distribution in a 36-Tube Bundle, Square Array, Horizontal Position. Predicted temperatures (°C) are shown in the lower half of the circles. Q = 0.0434 w/cm of tube; average wall temperature = 50.2°C.

UNCLASSIFIED
ORNL-LR-DWG. 78744

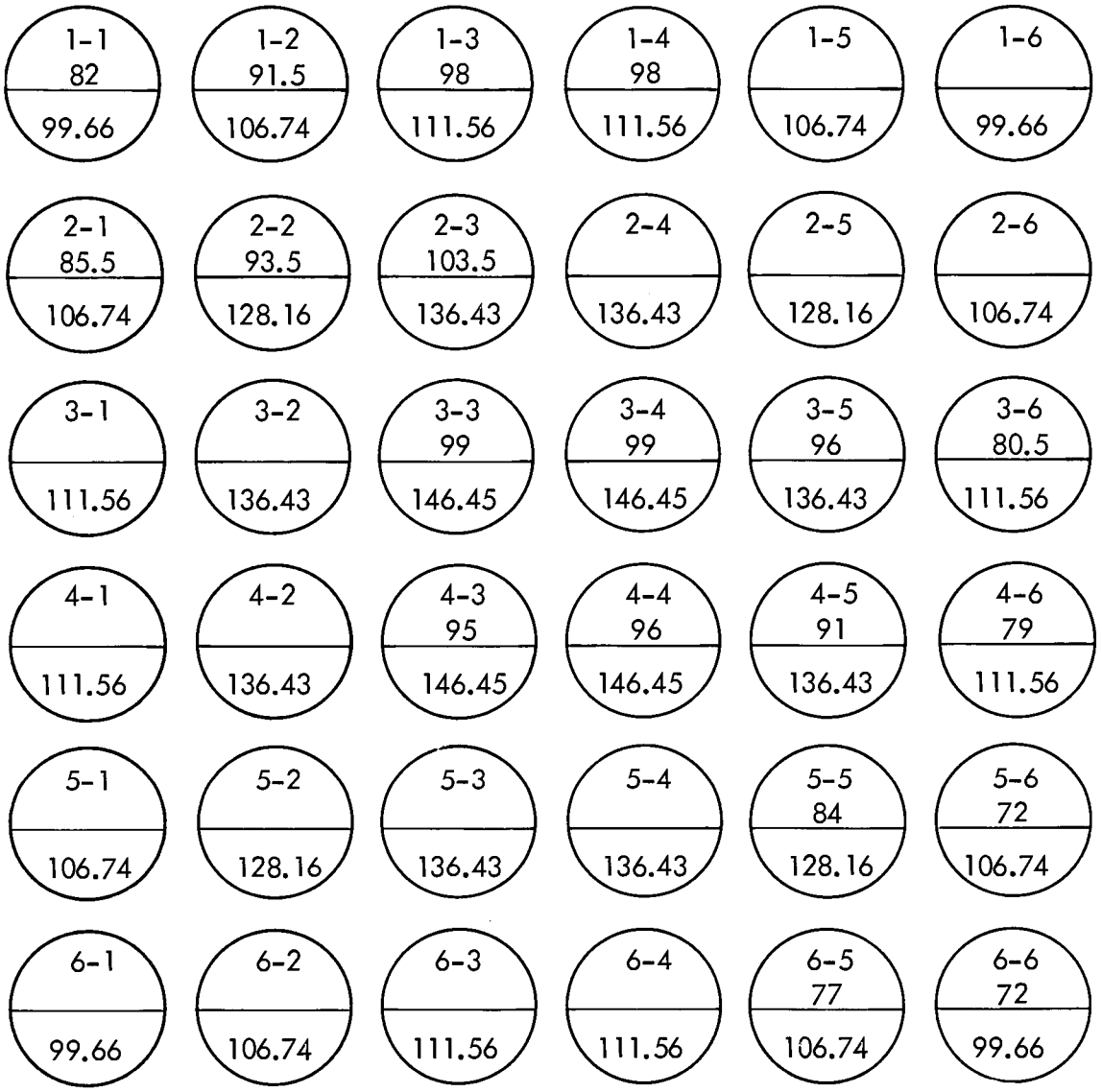

Fig. 27. Predicted and Experimental Temperature Distribution in a 36-Tube Bundle, Square Array, Horizontal Position. Predicted temperatures (°C) are shown in the lower half of the circles. Q = 0.0268 w/cm of tube; average wall temperature = 39.8°C.

UNCLASSIFIED
ORNL-LR-DWG. 78745

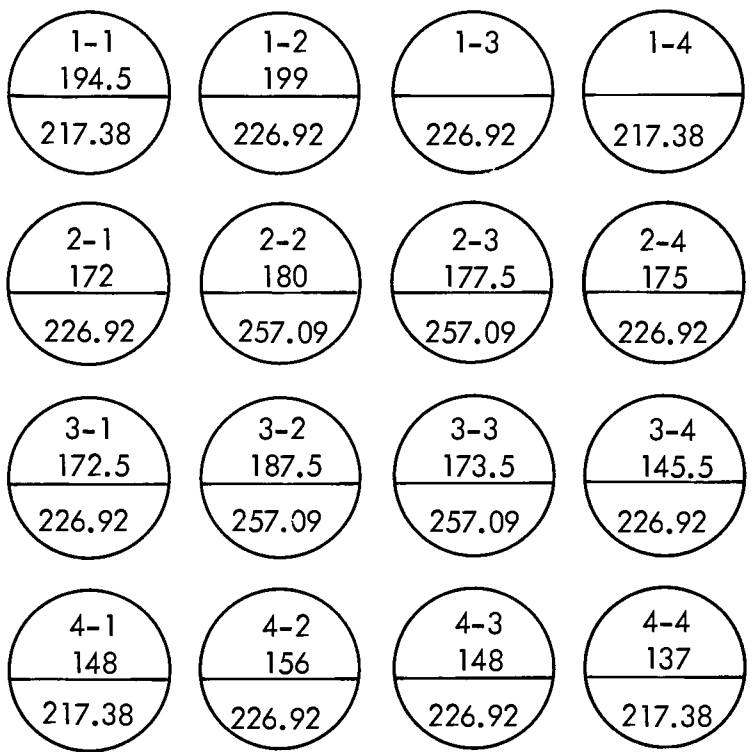

Fig. 28. Predicted and Experimental Temperature Distribution in a 16-Tube Bundle, Square Array, Horizontal Position. Predicted temperatures (°C) are shown in the lower half of the circles. Q = 0.150 w/cm of tube; average wall temperature = 57.5°C.

UNCLASSIFIED
ORNL-LR-DWG. 78746

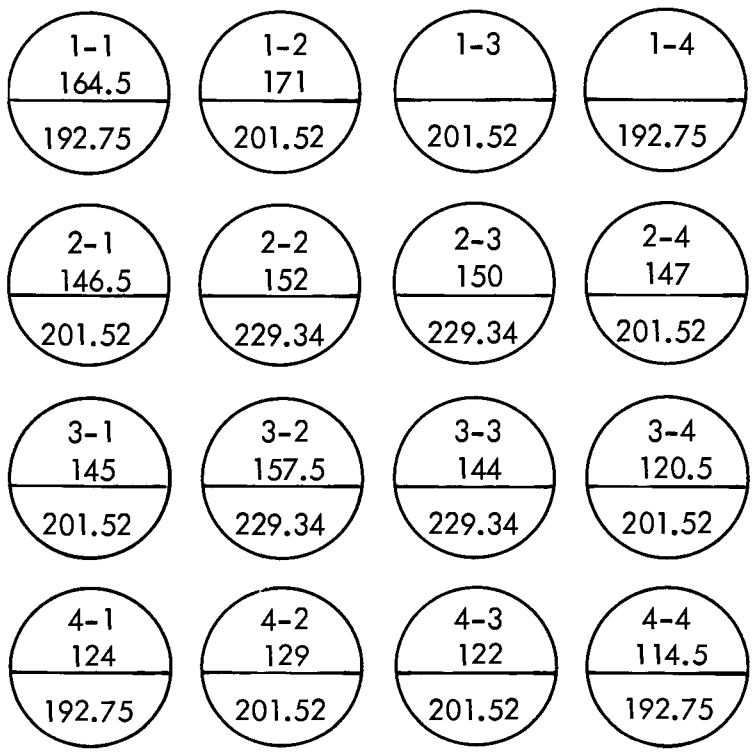

Fig. 29. Predicted and Experimental Temperature Distribution in a 16-Tube Bundle, Square Array, Horizontal Position. Predicted temperatures (°C) are shown in the lower half of the circles. Q = 0.118 w/cm of tube; average wall temperature = 50.5°C.

UNCLASSIFIED
ORNL-LR-DWG. 78747

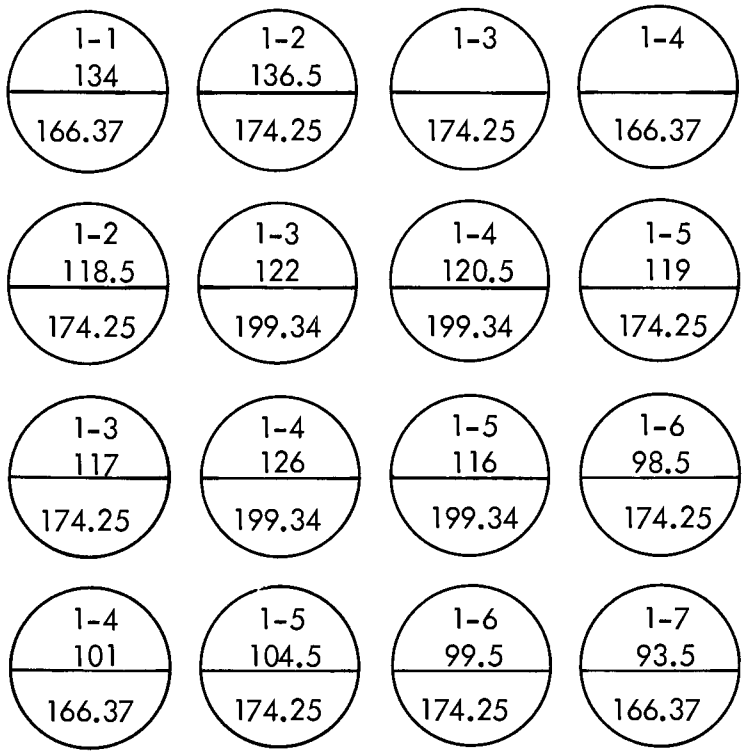

Fig. 30. Predicted and Experimental Temperature Distribution in a 16-Tube Bundle, Square Array, Horizontal Position. Predicted temperatures (°C) are shown in the lower half of the circles. Q = 0.0888 w/cm of tube; average wall temperature = 44.0°C.

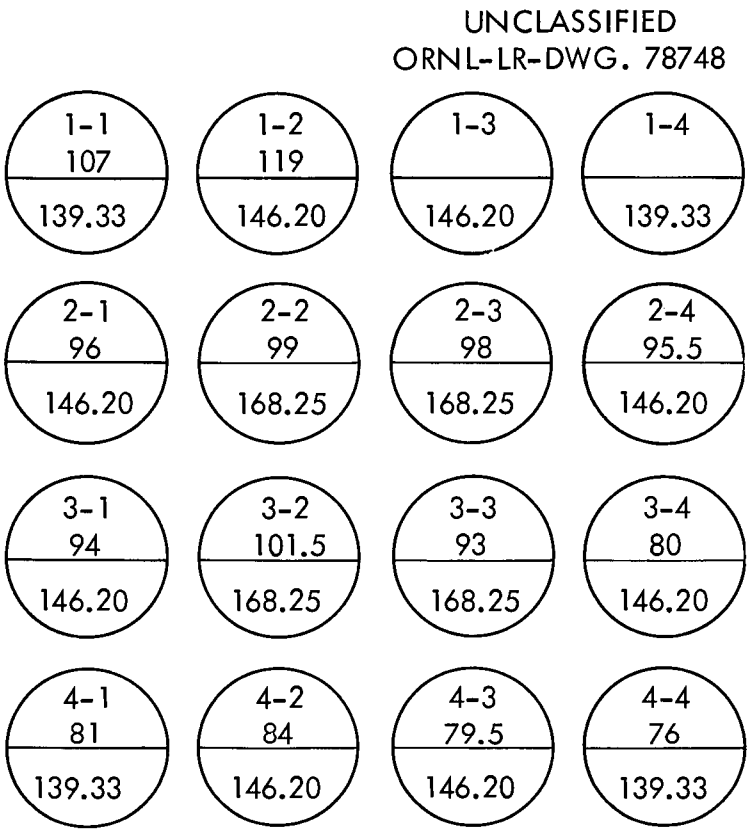

Fig. 31. Predicted and Experimental Temperature Distribution in a 16-Tube Bundle, Square Array, Horizontal Position. Predicted temperatures (°C) are shown in the lower half of the circles. Q = 0.0639 w/cm of tube; average wall temperature = 38.0°C.

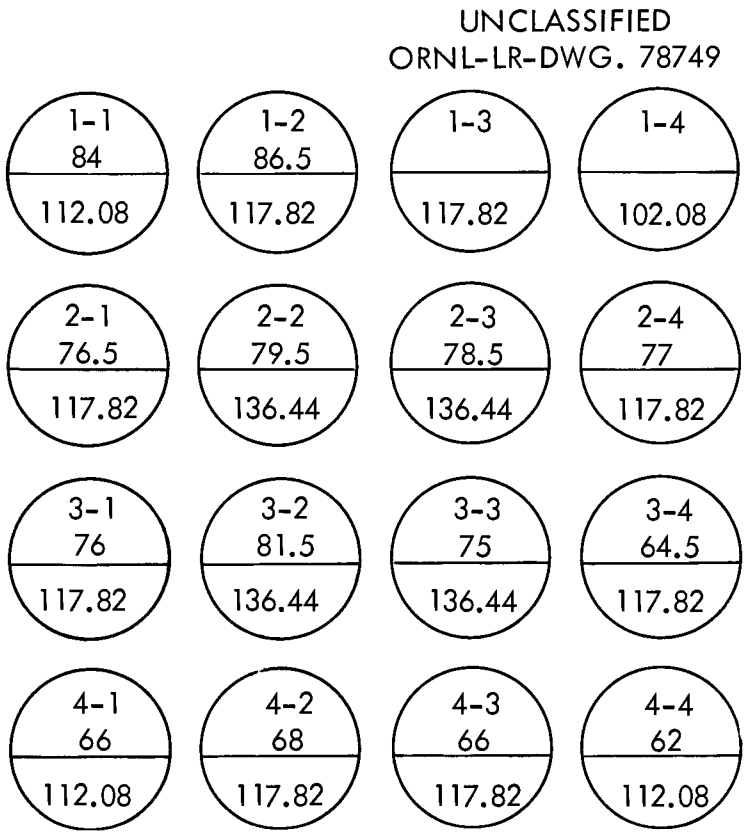

Fig. 32. Predicted and Experimental Temperature Distribution in a 16-Tube Bundle, Square Array, Horizontal Position. Predicted temperatures (°C) are shown in the lower half of the circles. Q = 0.0434 w/cm of tube; average wall temperature = 32.5°C.

UNCLASSIFIED
ORNL-LR-DWG. 78750

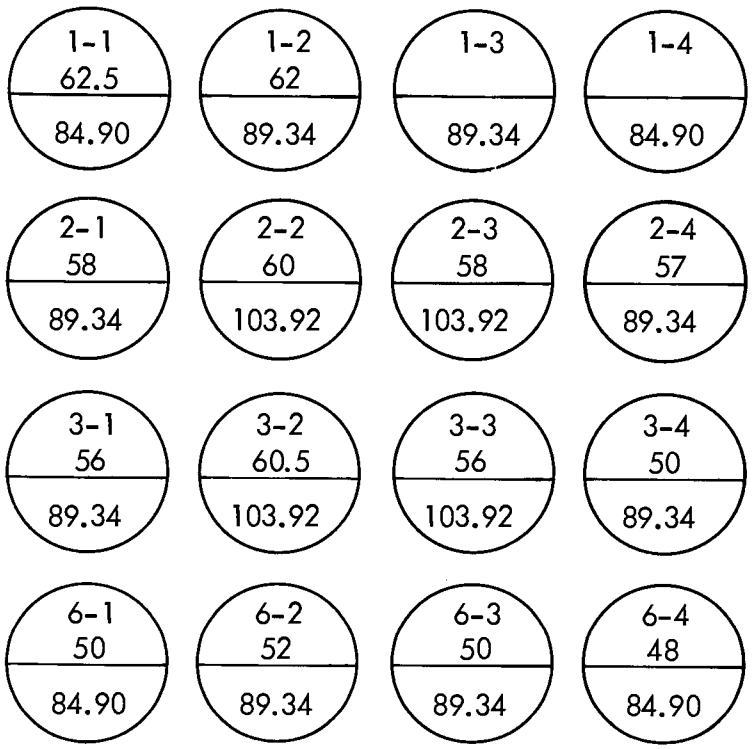

Fig. 33. Predicted and Experimental Temperature Distribution in a 16-Tube Bundle, Square Array, Horizontal Position. Predicted temperatures (°C) are shown in the lower half of the circles. Q = 0.0268 w/cm of tube; average wall temperature = 28.0°C.

UNCLASSIFIED
ORNL-LR-DWG. 78751

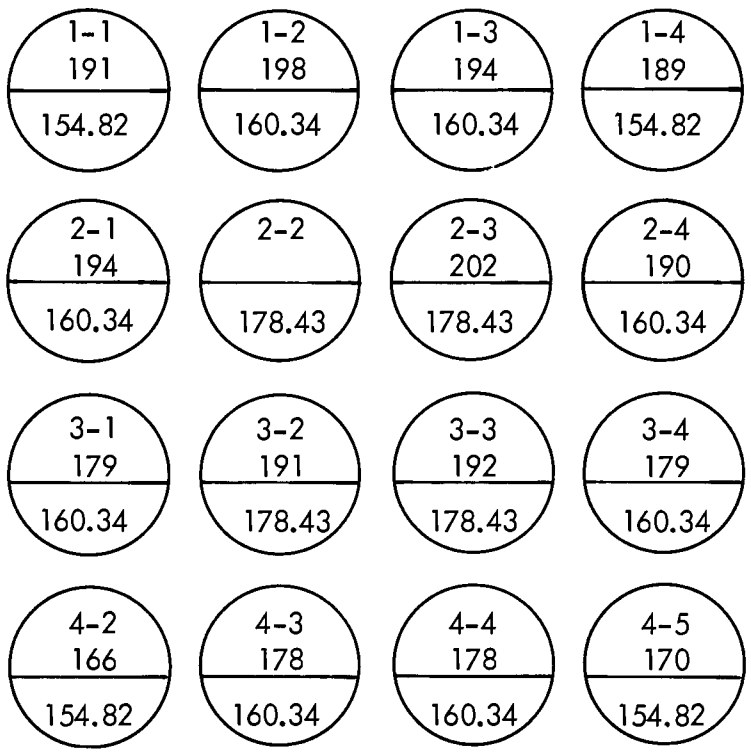

Fig. 34. Predicted and Experimental Temperature Distribution in a 16-Tube Bundle, Square Array, Horizontal Position in a 6-in. Cask. Predicted temperatures (°C) are shown in the lower half of the circles. Q = 0.057 w/cm of tube; average wall temperature = 83.0°C.

UNCLASSIFIED
ORNL-LR-DWG. 78752

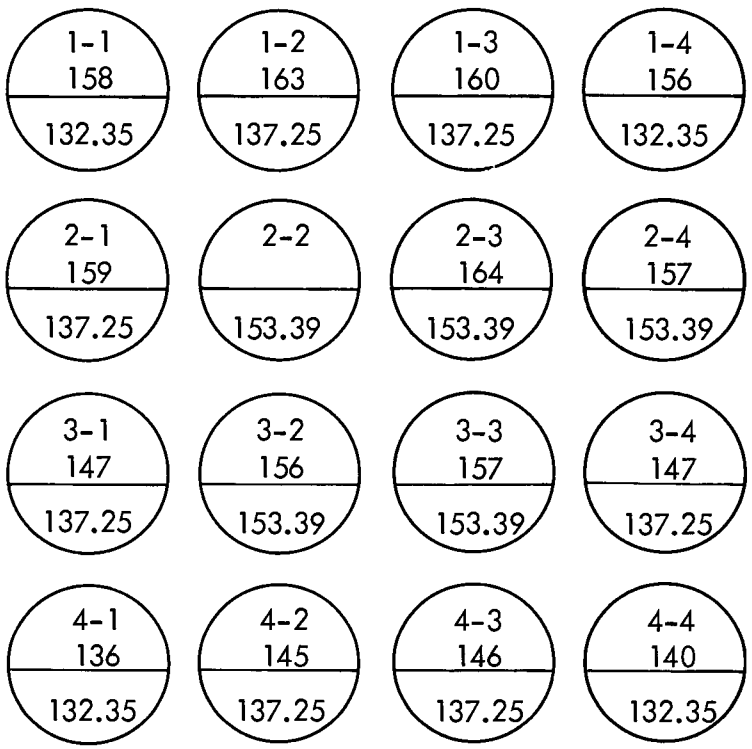

Fig. 35. Predicted and Experimental Temperature Distribution in a 16-Tube Bundle, Square Array, Horizontal Position in a 6-in. Cask. Predicted temperatures (°C) are shown in the lower half of the circles. Q = 0.043 w/cm of tube; average wall temperature = 70.0°C.

UNCLASSIFIED
ORNL-LR-DWG. 78753

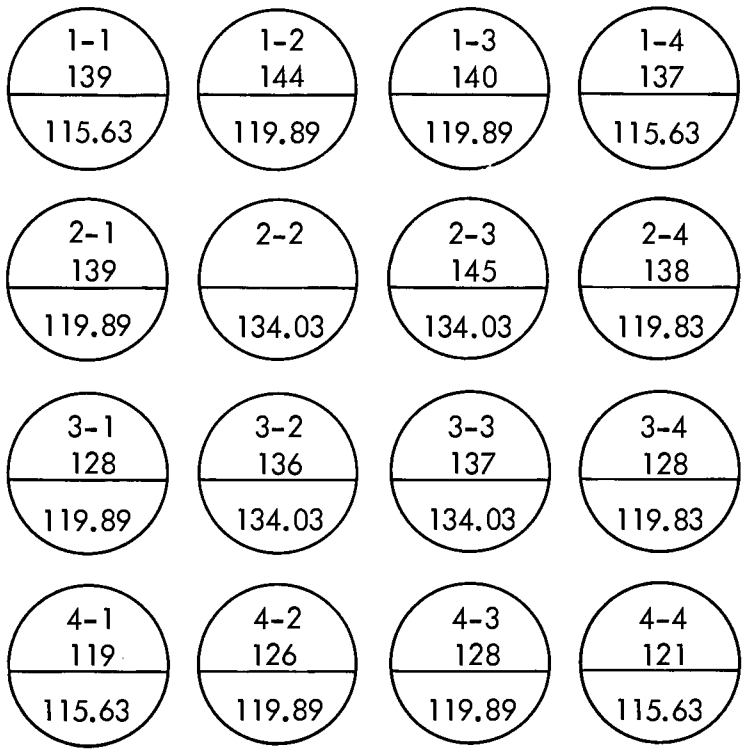

Fig. 36. Predicted and Experimental Temperature Distribution in a 16-Tube Bundle, Square Array, Horizontal Position in a 6-in. Cask. Predicted temperatures (°C) are shown in the lower half of the circles. Q = 0.0329 w/cm of tube; average wall temperature = 63.0°C.

UNCLASSIFIED
ORNL-LR-DWG. 78754

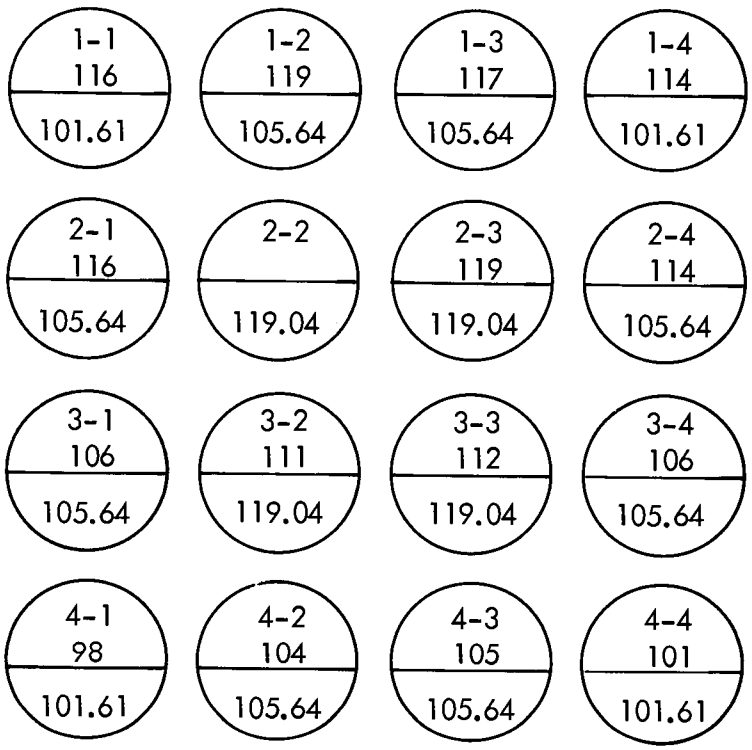

Fig. 37. Predicted and Experimental Temperature Distribution in a 16-Tube Bundle, Square Array, Horizontal Position in a 6-in. Cask. Predicted temperatures (°C) are shown in the lower half of the circles. Q = 0.0279 w/cm of tube; average wall temperature = 52.0°C.

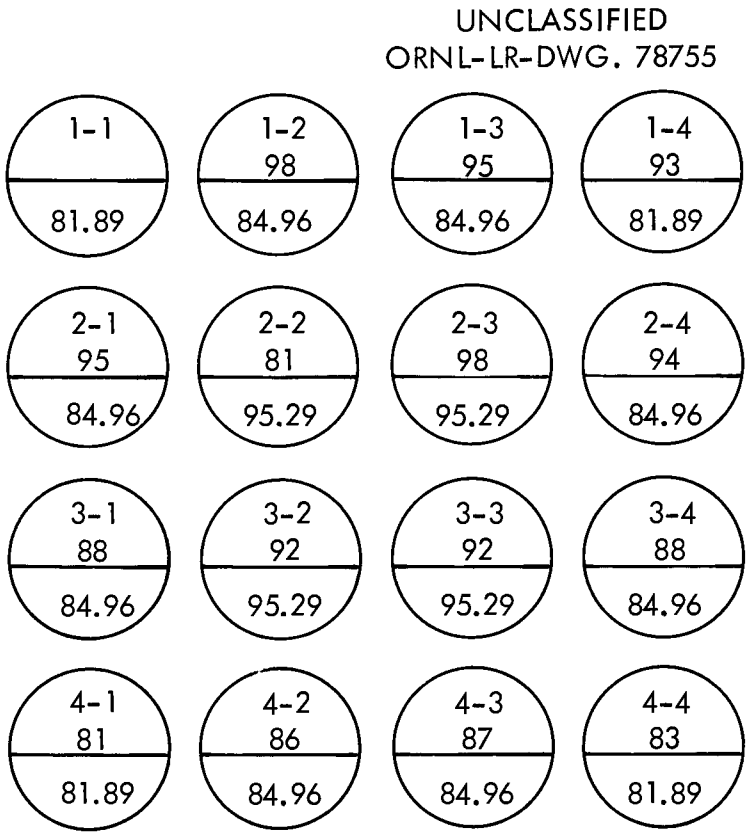

Fig. 38. Predicted and Experimental Temperature Distribution in a 16-Tube Bundle, Square Array, Horizontal Position in a 6-in. Cask. Predicted temperatures (°C) are shown in the lower half of the circles. Q = 0.018 w/cm of tube; average wall temperature = 46.0°C.

UNCLASSIFIED
ORNL-LR-DWG. 78756

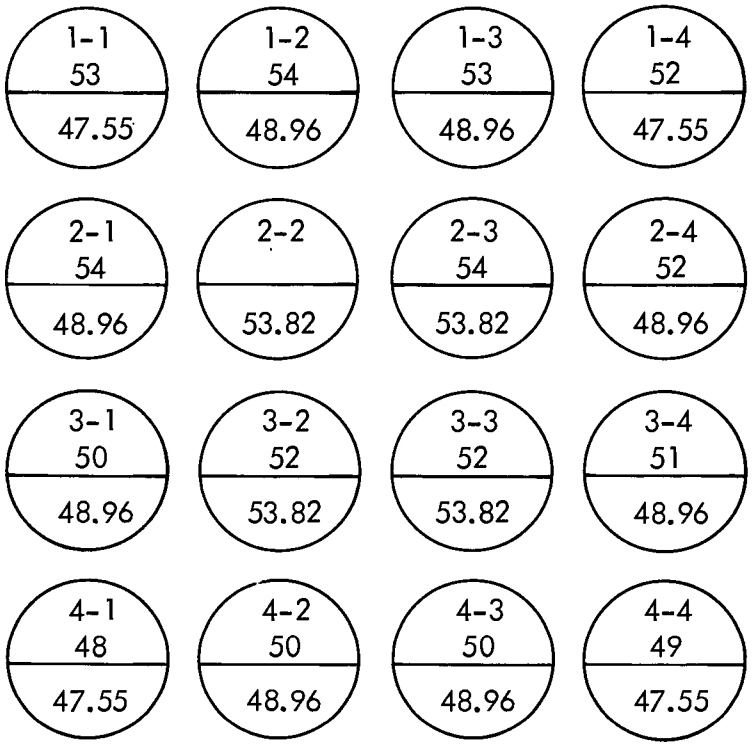

Fig. 39. Predicted and Experimental Temperature Distribution in a 16-Tube Bundle, Square Array, Horizontal Position in a 6-in. Cask. Predicted temperatures (°C) are shown in the lower half of the circles. Q = 0.00604 w/cm of tube; average wall temperature = 32.5°C.

UNCLASSIFIED
ORNL-LR-DWG. 78757

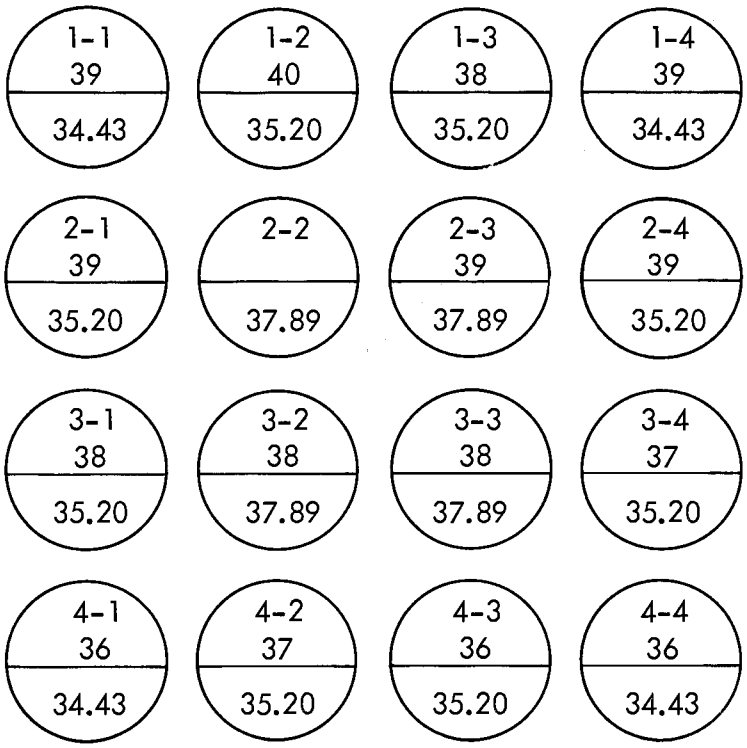

Fig. 40. Predicted and Experimental Temperature Distribution in a 16-Tube Bundle, Square Array, Horizontal Position in a 6-in. Cask. Predicted temperatures (°C) are shown in the lower half of the circles. Q = 0.0029 w/cm of tube; average wall temperature = 26.5°C.

5. CONCLUSIONS AND RECOMMENDATIONS

Temperature distributions in spent fuel elements during shipping were studied by using electrically heated tube bundles and simulated shipping casks. A calculational procedure based upon transfer of heat by radiation has been shown to give good predictions of the measured temperature distributions for the conditions likely to be of interest in shipping spent fuels (closely packed bundles with high heat generation rates and temperatures). In the cases where the procedure is not applicable (loosely packed bundles with low heat generation rates and temperatures), the procedure will give conservative (high) values for the temperatures.

The calculations have been coded and can be made very quickly on a high-speed computer. They should be valuable to a cask designer who would like to quickly compare the heat transfer properties of several proposed cask designs or to a designer making economic and safety studies of proposed shipments of spent fuel. In addition, the method may be adaptable to other types of arrays.

6. REFERENCES

1. D. C. Hamilton and W. B. Morgan, Radiant-Interchange Configuration Factors, NACA-2836 (1952).
2. V. Y. Frenkel, Inzhenero-Fizichiskii zhurnal 3(4), 85-9 (1960).
3. W. H. McAdams, Heat Transmission, 3d ed., 1954.
4. M. Jakob, Heat Transfer, vol II, 1957.

7. APPENDIX A

FORTRAN Code

Table A.1 shows the FORTRAN form of the calculations used to obtain the predicted temperature distributions. The calculations require eight input variables. In this study, many conditions remained unchanged during several runs, and it was convenient to place each of these numbers on

Table A.1. FORTRAN Code

```
C       TUBE BUNDLE RADIATION CODE
        DIMENSION T(50,50),F(5),FN(5)
   30   READINPUTTAPE10,20,NT,TW,Q,E,R,(F(J),J#1,3)
        NS#NT+2
        NC#(NT/2)+2
        NZ#NZ+1
        X#2.0*((1.0/E)-1.0)
        F(4)#F(1)+2.0*F(2)+4.0*F(3)
        F(5)#2.0*F(1)+3.0*F(2)+6.0*F(3)
        DO33M#1,5
   33   FN(M)#1.0/((1.0/F(M))+X)
        TW#TW+273.0
        TW#(TW*TW)*(TW*TW)
        C#1000000.
        L#NS+2
        DO12M#1,L
        DO13N#1,L
   13   T(M,N)#TW
   12   CONTINUE
        X#(.356435E-10)*R
        DO14M#1,5
   14   FN(M)#X*FN(M)
        FC#FN(5)+2.0*(FN(1)+FN(3))+FN(2)
        FT#4.0*(FN(1)+FN(2)+(2.0*FN(3)))
        FW#FN(4)+2.0*(FN(1)+FN(2))+4.0*FN(3)
    9   TC#T(NC,NC)
        X#FN(5)*TW+FN(1)*T(3,4)*2.0+FN(2)*T(4,4)+2.0*FN(3)*T(4,5)
        T(3,3)#(Q+X)/FC
        T(3,NS)#T(3,3)
        T(NS,3)#T(3,3)
        T(NS,NS)#T(3,3)
        DO31N#4,NC
        X#FN(4)*TW+FN(1)*(T(3,N+1)+T(3,N-1))+FN(2)*(T(4,N+1)+T(4,N-1))
       1+FN(3)*(T(4,N+2)+T(4,N-2)+T(5,N+1)+T(5,N-1))
        T(3,N)#(Q+X)/FW
        M#L-N+1
        T(3,M)#T(3,N)
        T(NS,M)#T(3,N)
        T(NS,N)#T(3,N)
        T(N,3)#T(3,N)
        T(N,NS)#T(3,N)
        T(M,3)#T(3,N)
   31   T(M,NS)#T(3,N)
        DO7M#4,NC
        DO6N#M,NC
        X#FN(1)*(T(M,N+1)+T(M,N-1)+T(M+1,N)+T(M-1,N))
        X#X+FN(2)*(T(M+1,N+1)+T(M-1,N-1)+T(M+1,N-1)+T(M-1,N+1))
        X#X+FN(3)*(T(M+1,N+2)+T(M+2,N+1)+T(M-1,N-2)+T(M-2,N-1))
        X#X+FN(3)*(T(M-1,N+2)+T(M+1,N-2)+T(M-2,N+1)+T(M+2,N-1))
        T(M,N)#(Q+X)/FT
        T(N,M)#T(M,N)
        J#L-M+1
        K#L-N+1
        T(J,K)#T(M,N)
        T(K,J)#T(M,N)
        T(M,K)#T(M,N)
        T(J,N)#T(M,N)
        T(N,J)#T(M,N)
```

Table A.1. FORTRAN Code (Cont'd)

```
 6 T(K,M)#T(M,N)
 7 CONTINUE
   TC#ABSF(T(NC,NC)-TC)
   IF(TC-C)8,8,9
 8 WRITEOUTPUTTAPE9,21
   TW#SQRTF(SQRTF(TW))-273.0
   WRITEOUTPUTTAPE9,22,NT,TW,Q,E,R
   WRITEOUTPUTTAPE9,23
   WRITEOUTPUTTAPE9,26,F(1),F(2),F(3)
   WRITEOUTPUTTAPE9,25
   DO10M#3,NS
   L#M-2
   DO11N#3,NS
   J#N-2
   T(M,N)#SQRTF(SQRTF(T(M,N)))-273.0
11 WRITEOUTPUTTAPE9,24,L,J,T(M,N)
10 CONTINUE
   GOTO30
20 FORMAT(I3/(E14.6))
21 FORMAT(65H1     NO TUBES   WALL TEMP           Q                E
  1         R)
22 FORMAT(1H I9,4E14.6)
23 FORMAT(38H         F1              F2              F3)
26 FORMAT(1H 3E14.6)
25 FORMAT(25H TEMPERATURE DISTRIBUTION/24H TUBE NO   TEMP DEGREES C)
24 FORMAT(1H I4,I5,F10.2)
   END(1,1,0,0,0,0,0,0,0,0,0,0,0,0,0)
```

separate cards (starting in column 1). Table A.2 shows the order and form in which the code of Table A.1 calls for these data. After a set of calculations has been completed, the code will call for another set of data. Finally, after no more data are available, the code will EXIT (on the Oak Ridge monitor). If these units and input method are satisfactory for a similar problem, copies of either the FORTRAN or compiled binary decks can be obtained from the author. For an 8 x 8 array, less than 15 sec were required to obtain a steady-state temperature distribution. This time, however, will increase more than linearly with the number of tubes in the array.

Table A.2. Input Variables

Variable	Symbol	Unit	Format Field Type and Width
No. of tubes in each row	NT	Dimensionless	I 3
Wall Temperature	TW	°C	E 14.6
Heat Generation Rate	Q	Watts per centimeter of tube	E 14.6
Emissivity	E	Dimensionless	E 14.6
Tube Radius	R	cm	E 14.6
Adjacent configuration factor	F(1)	Dimensionless	E 14.6
Diagonal configuration factor	F(2)	Dimensionless	E 14.6
configuration factor	F(3)	Dimensionless	E 14.6

ORNL-3439
UC-38 - Engineering and Equipment
TID-4500 (19th ed., Rev.)

INTERNAL DISTRIBUTION

1. Biology Library
2-3. Central Research Library
4. Reactor Division Library
5-6. ORNL - Y-12 Technical Library, Document Reference Section
7-25. Laboratory Records Department
26. Laboratory Records, ORNL R.C.
27. S. J. Ball
28. J. O. Blomeke
29. R. L. Bradshaw
30. J. C. Bresee
31. T. A. Butler
32. H. C. Claiborne
33. F. L. Culler
34. F. W. Davis
35. B. C. Finney
36. H. E. Goeller
37. C. E. Guthrie
38. Neil Hilvety
39. H. W. Hoffman
40. J. M. Holmes
41. G. W. Keilholtz
42. O. H. Klepper
43. T. Koizumi
44. J. A. Lane
45. C. E. Larson
46. H. A. McLain
47. J. R. McWherter
48. F. H. Neill
49. J. P. Nichols
50. J. Perona
51. R. A. Robinson
52. G. Samuels
53. W. F. Schaffer, Jr.
54. L. B. Shappert
55. M. J. Skinner
56. J. A. Swartout
57. J. W. Ullmann
58. C. D. Watson
59. J. S. Watson
60. G. M. Watson
61. Herman Weeren
62. A. M. Weinberg
63. M. E. Whatley
64. H. B. Whetsel
65. J. J. Katz (consultant)
66. T. H. Pigford (consultant)
67. C. E. Winters (consultant)
68. H. Worthington (consultant)

EXTERNAL DISTRIBUTION

69. Research and Development Division, AEC, ORO
70-572. Given distribution as shown in TID-4500 (19th ed., Rev.) under Engineering and Equipment category (75 copies - OTS)